Title

Discovery of Small Molecule Drugs against Crucial Proteins, Papain-like Protease (PLpro) and Non-structural protein 15 (Nsp15), from SARS-CoV-2 virus

Author

Bajaj, Teena

Publication Date

2024

Peer reviewed|Thesis/dissertation

Discovery of Small Molecule Drugs against Crucial Proteins, Papain-like Protease (PLpro) and Non-structural protein 15 (Nsp15), from SARS-CoV-2 virus

by

Teena Bajaj

A dissertation submitted in partial satisfaction of the

requirements for the degree of

Doctor of Philosophy

in

Comparative Biochemistry

in the

Graduate Division

of the

University of California, Berkeley

Committee in charge:

Professor Niren Murthy, Chair
Professor Fenyong Liu
Professor Daniel K. Nomura

Summer 2024

Discovery of Small Molecule Drugs against Crucial Proteins, Papain-like Protease (PLpro) and Non-structural protein 15 (Nsp15), from SARS-CoV-2 virus

Abstract

Discovery of Small Molecule Drugs against Crucial Proteins, Papain-like Protease (PLpro) and Non-structural protein 15 (Nsp15), from SARS-CoV-2 virus

by

Teena Bajaj

Doctor of Philosophy in Comparative Biochemistry

University of California, Berkeley

Professor Niren Murthy, Chair

The emergence and rapid spread of the severe acute respiratory syndrome coronavirus 2, SARS-CoV-2 (SCoV-2) caused catastrophic levels of morbidity in the world and presented the unmet need for treatments and drugs urgently. Small molecule therapeutics have tremendous potential to develop into antivirals and prevent the spread of infection. SCoV-2 genome encodes for 16 non-structural proteins (Nsps) that have been proven as potential target candidates. Two vital proteins, Papain-like protease (PLpro) (Papain-like protease, from Nsp3) and Non-structural protein 15 (Nsp15) were chosen as therapeutic targets to combat the SCoV-2 virus. PLpro is an essential protein that cleaves the polyprotein into its individual proteins to form a replication-transcription complex for viral replication and synthesis. On another hand, Nsp15 is a crucial protein that evades the host immune response by cleaving the viral RNA, therefore, Nsp15 inhibition stimulates the protective response. Both nsps are highly conserved proteins and the development of drugs against them could also act as an initial step for future coronavirus pandemics. To find the covalent inhibitors of PLpro and Nsp15, the electrophile library was screened against these two proteins using their respective fluorescent-based, high-throughput screening assay. To find the inhibitors against the PLpro, a chemical library was screened against the recombinantly purified PLpro using a fluorescent-based high throughput screening assay. One compound, based on mercaptopyrimidine inhibited PLpro invitro and SARS-CoV-2 viral replication in Vero E6 cells. This compound presented the first example of a thiol-targeted reversible covalent inhibitor of PLpro. In the case of Nsp15, an acrylamide-based electrophile library was screened to find cysteine-binding inhibitors. This discovered a new class of Nsp15 covalent inhibitors. This study not only discovered new covalent lead hits against crucial proteins from SCoV-2, but also a new platform to develop new potent drugs against coronaviruses for future pandemics.

Dedication

To the millions of people who lost their lives and loved ones during the COVID-19 pandemic

Contents

List of Figures

Acknowledgments

To all the "Angels" on this beautiful planet who supported me in one way or another during these seven years of my journey of doctoral studies. Thank you for all of your support along the way. I am deeply grateful to have you all in my life. "Thank You" !!

Chapter 1

Introduction

The emergence and rapid spread of the SARS-CoV-2 (SCoV-2) virus marked the beginning of the COVID-19 pandemic, which originated in Wuhan, China in December 2019. COVID-19 patients showed symptoms of shortness of breath, fever, cough, and loss of taste and smell. This contagious virus surged the cases dramatically with thousands of new infections being reported daily[1]. World Health Organization (WHO) declared the novel coronavirus outbreak a pandemic in early March 2020. The pandemic had profound and far-reaching impacts on global health systems, economies, and daily life[2]. The devastating toll on human life has been immense; as of mid-2024, estimates over 7 million people have died worldwide due to COVID-19 (https://www.who.int/publications/m/item/covid-19-epidemiological-update—19-january-2024). This catastrophic global health crisis has highlighted the urgent need for effective antiviral drugs and therapies to manage COVID-19 and alleviate its symptoms, driving intense research and development efforts to combat the virus and mitigate its impact on public health.

1.1 Description of SCoV-2

SCoV-2 is an enveloped, positive-sense single-stranded RNA virus that belongs to the betacoronavirus genus, which also includes SARS-CoV and MERS-CoV. SCoV-2 has the largest RNA virus genome approximately 30kb in length[3]. The SCoV-2 genome encodes several key proteins essential for the virus's structure and replication. There are 5 structural and 16 non-structural proteins. The structural proteins play vital roles in the ability of virus to infect host cells, assemble new viral particles, and facilitate their release. These proteins include the spike (S) protein, envelope (E) protein, membrane (M) protein, and nucleocapsid (N) protein[4]. The spike protein is particularly significant as it mediates the virus's attachment to the angiotensin-converting enzyme 2 (ACE2) receptor on host cells, initiating the infection process.[5] The envelope and membrane proteins contribute to the formation and stability of the viral envelope, while the nucleocapsid protein packages the viral RNA into a protective nucleocapsid, essential for the assembly of new virions[6].

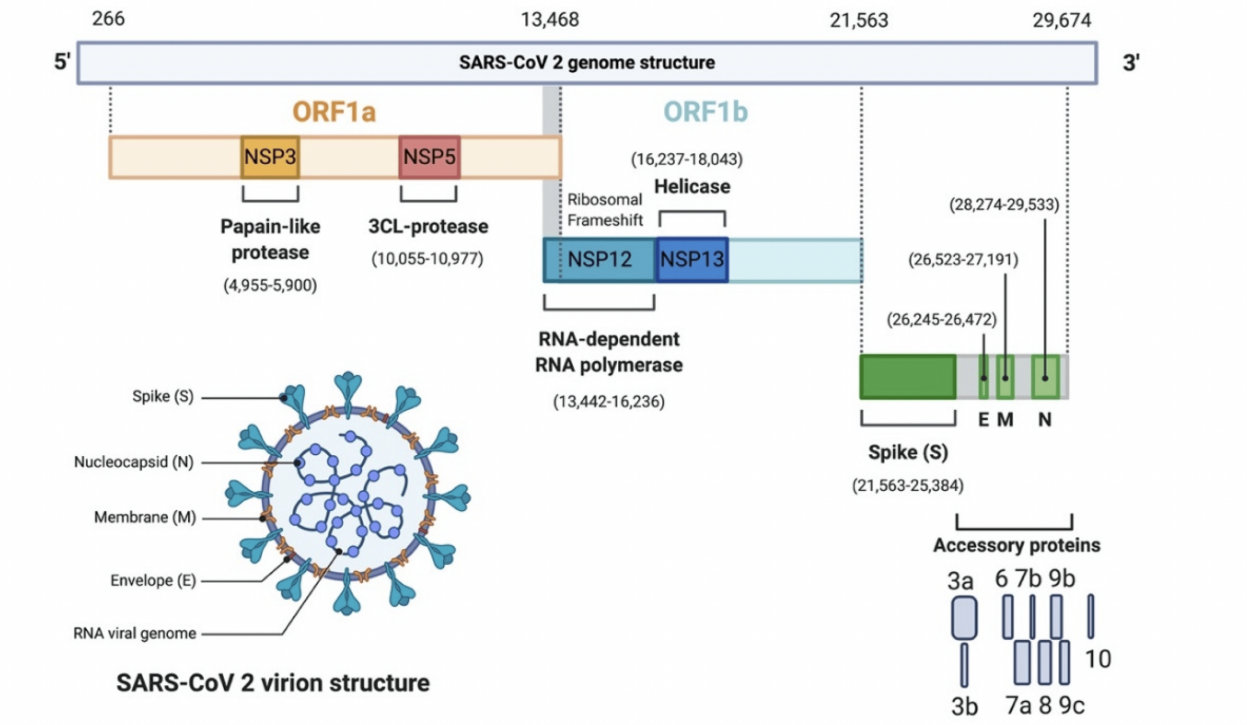

Figure 1.1: Scheme of the SCoV-2 genome along with the most critical reported diversities in its different parts, as well as the general structure of the SCoV-2.[7]

In addition to the structural proteins, SCoV-2 encodes non-structural proteins that are primarily involved in the replication and transcription of the viral genome. These non-structural proteins are crucial for various functions within the virus's life cycle, including the processing of polyproteins, RNA synthesis, and the assembly of the replication-transcription complex. Notable non-structural proteins include the RNA-dependent RNA polymerase (RdRp), which is essential for viral RNA replication, and various proteases such as the main protease (Mpro) and the papain-like protease (PLpro), which process viral polyproteins into functional units necessary for viral replication[8]. Non-structural proteins are critical for the replication of the viral genome and for evading the host immune system. By targeting these proteins, researchers aim to inhibit the virus's replication and enhance immune responses, thereby developing effective therapies and preventive measures against COVID-19. The comprehensive study of these proteins allows for the design of drugs and vaccines that can specifically disrupt viral processes and improve overall treatment outcomes.

1.2 Small molecules therapeutics

Small molecule therapeutics has presented itself as a great solution for treatments of infectious diseases. Small molecule therapy for COVID-19 represents a crucial advancement in the ongoing fight against the pandemic, complementing existing vaccination efforts by providing effective treatment options for those already infected with the virus. These therapies are important for several reasons. Firstly, they offer a vital solution for managing active infections, addressing the gap left by vaccines, which are designed primarily to prevent disease rather than treat it once it has begun. Small molecules, such as antivirals, can reduce the viral load in patients, thereby mitigating the severity of the disease and preventing progression to more serious stages. This capability is especially critical in managing severe cases and preventing hospitalization, thereby alleviating the burden on healthcare systems.[15] Additionally, small molecules can be adapted to target various viral mechanisms, making them potentially effective against different variants of SCoV-2, which may evade the immune response elicited by vaccines. Furthermore, the oral administration of many small-molecule drugs enhances their accessibility and convenience compared to intravenous treatments, facilitating widespread use, particularly in outpatient settings. Their production is often more scalable and cost-effective than biologics, aiding in rapid distribution and availability, especially in resource-limited areas. Small molecule therapies also serve as an essential alternative for individuals who are unable to receive vaccines due to medical conditions or other constraints, and they offer critical options for immunocompromised patients who may not respond well to vaccination.[16] Additionally, these therapies can help address drug resistance by targeting novel aspects of the viral life cycle, thereby providing a dynamic tool for managing evolving strains of the virus. Overall, small molecule therapies are a pivotal component of the comprehensive strategy to control COVID-19, working in tandem with vaccines and other treatments to enhance public health outcomes and manage the pandemic more effectively.

The key targets for therapeutic intervention in combating COVID-19 include viral entry, viral replication, and immune modulation. To prevent viral entry, strategies focus on blocking the spike protein of SARS-CoV-2 from binding to the ACE2 receptor on host cells, utilizing monoclonal antibodies and entry inhibitors. For viral replication, inhibiting crucial enzymes such as RNA-dependent RNA polymerase (RdRp), proteases like main protease (Mpro), and papain-like protease (PLpro) is essential. Additionally, Nsp15, an endoribonuclease involved in RNA processing and immune evasion, is another critical target for antiviral drug development. Immune modulation involves managing the host's immune response to prevent severe disease; corticosteroids like dexamethasone are used to reduce inflammation and moderate cytokine storms, which can lead to severe outcomes. By addressing these targets, therapeutic strategies aim to disrupt the virus's life cycle and mitigate the inflammatory response, improving overall patient outcomes.

Remdesivir, an antiviral drug, targets the RNA-dependent RNA polymerase (RdRp), inhibiting viral RNA replication. Paxlovid, a combination of nirmatrelvir and ritonavir, acts as a protease inhibitor, blocking the main protease (Mpro) essential for viral polyprotein processing. Molnupiravir, another antiviral, interferes with the RNA replication process by

introducing errors into the viral RNA. Dexamethasone, a corticosteroid, modulates the immune response by reducing inflammation and controlling cytokine storms. Together, these drugs represent a multifaceted approach to managing COVID-19, targeting viral entry, replication, and the inflammatory response to improve patient outcomes.

However, small molecule inhibitors still need further development. Firstly, developing small molecules that effectively target SCoV-2 and its variants is complex due to the virus's ability to rapidly mutate. Variants may alter the structure of viral proteins, making it difficult for drugs designed against earlier strains to remain effective.[17] Secondly, the mechanisms of action for many potential small molecules are still under investigation, and ensuring their safety and efficacy requires extensive clinical testing. Additionally, achieving optimal drug delivery and minimizing side effects are significant hurdles. Many small molecules show promise in preclinical studies but fail to translate into effective treatments due to issues like poor bioavailability or off-target effects. Furthermore, there is a need to address the challenge of drug resistance, which can arise with widespread use of antiviral therapies. The development of new small molecules must also contend with the complexity of the human immune response and the need for drugs that can work in conjunction with other treatments, such as vaccines and monoclonal antibodies[18].Given these factors, ongoing research and drug discovery are essential to identify and develop small molecule therapies that are safe, effective, and adaptable to emerging viral variants.

1.3 Non-structural proteins as therapeutic targets

In this essay, we will focus specifically on two proteases, papain-like protease (PLpro) and Nsp15, as key targets for therapeutic intervention. PLpro plays a crucial role in the viral life cycle by processing viral polyproteins and modulating the host immune response, making it a significant target for drug development. Similarly, Nsp15, an endonuclease enzyme, is involved in RNA processing and viral replication, presenting another important target for antiviral therapy. By targeting these proteases, we can explore potential therapeutic strategies to inhibit viral replication and enhance the treatment of COVID-19.

Papain-like protease (PLpro)

PLpro structurally is part of the larger non-structural protein 3 (nsp3) and is named for its structural similarity to papain, a protease enzyme. The enzyme has a catalytic triad consisting of cysteine, histidine, and aspartate residues, which are crucial for its protease activity. PLpro contains a ubiquitin-like domain and a thumb-palm-fingers domain, with the latter housing the catalytic site. Functionally, PLpro cleaves the viral polyprotein at three specific sites to release functional non-structural proteins (nsps), which are essential for the formation of the viral replication-transcription complex (RTC). PLpro also has deubiquitinating and deISGylating activities, meaning it can remove ubiquitin and ISG15 (interferon-stimulated gene 15) from host cell proteins. This helps the virus evade the host immune response

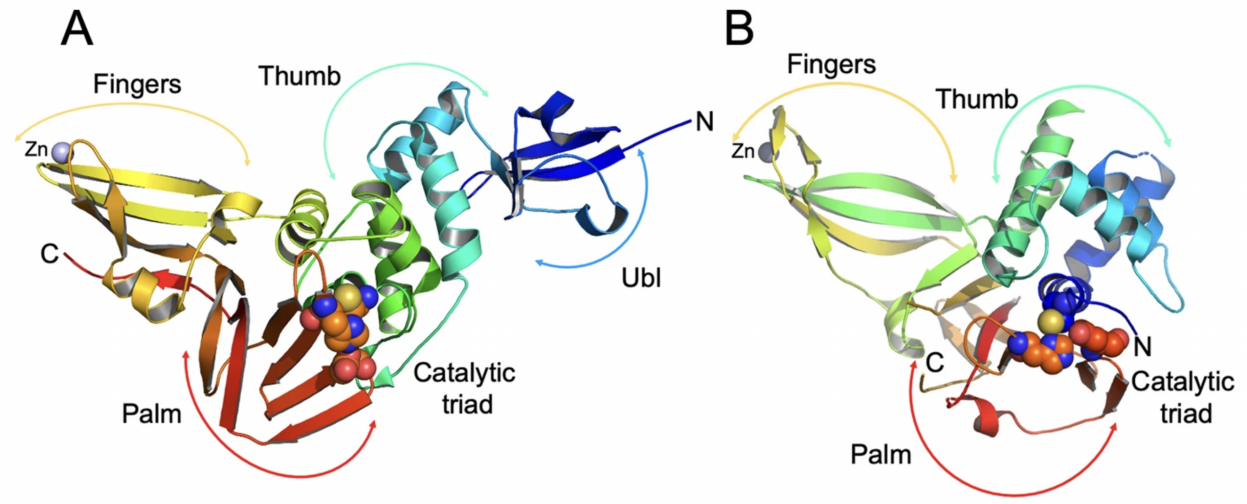

Figure 1.2: Secondary structure of PLpro.[21]

by preventing the degradation of viral proteins and modulating the host immune signaling pathways, However, due to its restricted substrate binding pocket, developing inhibitors for PLpro have been challenging.[19] The existing PLpro small molecule drug, GRL0617's primary benefit lies in its targeted action, effectively disrupting the viral replication cycle by inhibiting a crucial enzyme involved in processing viral polyproteins and evading the host immune response.[20] This specificity can potentially reduce viral load and disease severity, and as an oral small molecule, GRL0617 offers convenience and improved patient compliance. However, challenges include the potential for developing drug resistance, issues with specificity where the inhibitor might affect similar host proteases, and pharmacokinetic concerns such as drug absorption and metabolism. Additionally, its efficacy in advanced disease stages may be limited, necessitating ongoing research to address these issues and optimize its therapeutic potential.

Non-structural protein 15 (Nsp15)

Nsp15, or non-structural protein 15, is a critical component of the SCoV-2 virus and plays a pivotal role in its life cycle and interaction with the host immune system.[22] Structurally, Nsp15 is an endoribonuclease classified within the Nidoviral endoribonuclease specific for uridylate (NendoU) family. This protein is characterized by its three main domains: an N-terminal domain, a middle domain, and a C-terminal catalytic domain. The C-terminal catalytic domain is particularly significant as it contains the conserved residues essential for the protein's endoribonuclease activity. This activity is crucial for the enzyme's function in cleaving RNA substrates at uridine residues, resulting in the production of 2'-3'-cyclic phosphodiester and 5'-hydroxyl termini.[23]

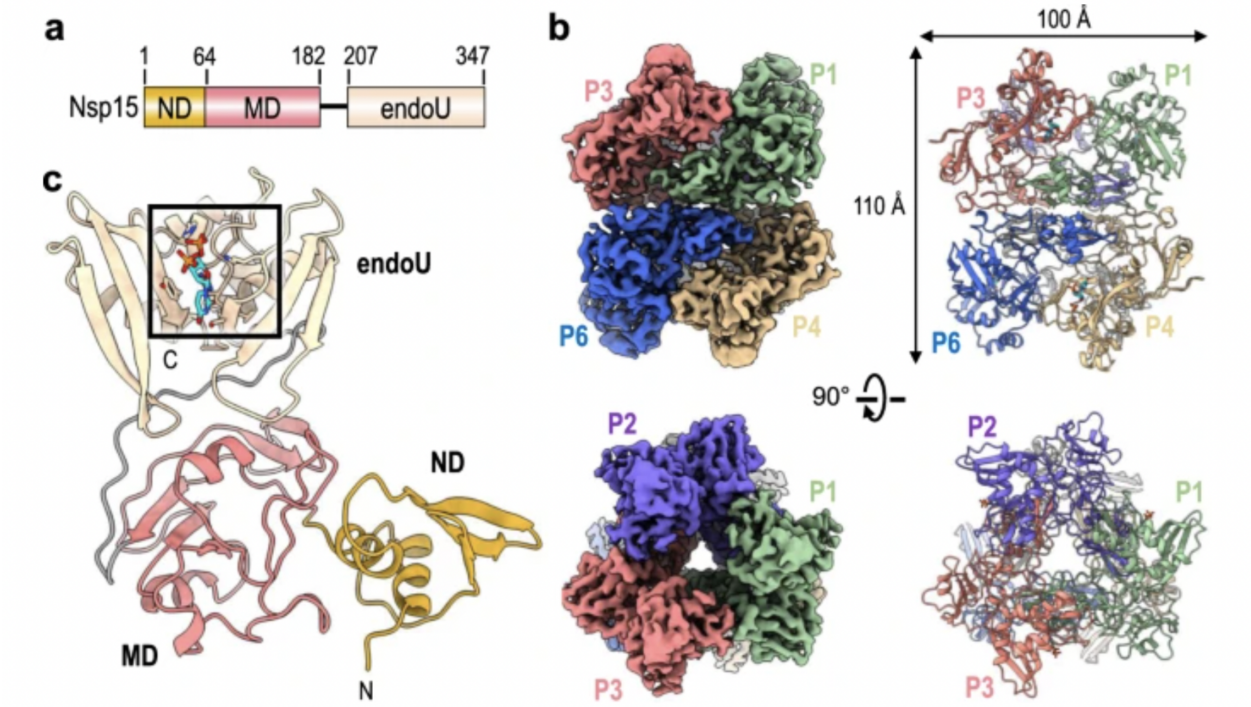

Figure 1.3: Structure of Nsp15. [26]

Functionally, Nsp15's endoribonuclease activity is integral to processing viral RNA intermediates during the replication cycle of SARS-CoV-2. By cleaving RNA substrates, Nsp15 prevents the accumulation of RNA fragments that could otherwise be detected by host immune sensors such as MDA5 and RIG-I.[24] This activity is crucial for the virus to evade detection by the host's innate immune system, enabling it to persist and replicate more efficiently. Targeting Nsp15 offers a promising therapeutic strategy, as small molecule inhibitors can disrupt this vital aspect of viral replication and bolster the host immune response. Hexachlorophene and IPA-3 are covalent inhibitor against Nsp15 with the potential to inhibit viral replication. However, these compounds are promiscuous molecule that has ability to bind human proteins as well and not specific to Nsp15. The challenge of drugging Nsp15 still remains with an open platform to find an inhibitor ensuring the specificity of IPA-3 to avoid unintended interactions with host cellular processes, and optimizing its pharmacokinetic properties for effective dosing and minimal side effects. The efficacy of IPA-3 in treating advanced stages of COVID-19 also requires further validation through ongoing research.[25]

1.4 References

1. J. Li, S. Lai, G. F. Gao and W. Shi, *Nature*, 2021, **600**, 408-418.

2. S. Muralidar, S. V. Ambi, S. Sekaran and U. M. Krishnan, *Biochimie*, 2020, **179**, 85-100.

3. S. Kumar, R. Nyodu, V. K. Maurya and S. K. Saxena, *Coronavirus Disease 2019 (COVID-19)*, 2020, DOI: 10.1007/978-981-15-4814-7_3, 23-31.

4. P. S. Masters, *Adv Virus Res*, 2006, **66**, 193-292.

5. R. Poduri, G. Joshi and G. Jagadeesh, *Cell Signal*, 2020, **74**, 109721.

6. L. Alanagreh, F. Alzoughool and M. Atoum, *Pathogens*, 2020, **9**.

7. A. Rahimi, A. Mirzazadeh and S. Tavakolpour, *Genomics*, 2021, **113**, 1221-1232.

8. Z. Jin, H. Wang, Y. Duan and H. Yang, *Biochem Biophys Res Commun*, 2021, **538**, 63-71.

9. M. Fabiani, M. Ramigni, V. Gobbetto, A. Mateo-Urdiales, P. Pezzotti and C. Piovesan, *Euro Surveill*, 2021, **26**.

10. C. Pawlowski, P. Lenehan, A. Puranik, V. Agarwal, A. J. Venkatakrishnan, M. J. M. Niesen, J. C. O'Horo, A. Virk, M. D. Swift, A. D. Badley, J. Halamka and V. Soundararajan, *Med*, 2021, **2**, 979-992.e978.

11. S. Nasreen, H. Chung, S. He, K. A. Brown, J. B. Gubbay, S. A. Buchan, D. B. Fell, P. C. Austin, K. L. Schwartz, M. E. Sundaram, A. Calzavara, B. Chen, M. Tadrous, K. Wilson, S. E. Wilson and J. C. Kwong, *medRxiv*, 2021, DOI: 10.1101/2021.06.28.21259420, 2021.2006.2028.21259420.

12. K. Lenart, R. Arcoverde Cerveira, F. Hellgren, S. Ols, D. J. Sheward, C. Kim, A. Cagigi, M. Gagne, B. Davis, D. Germosen, V. Roy, G. Alter, H. Letscher, J. Van Wassenhove, W. Gros, A.-S. Gallouët, R. Le Grand, H. Kleanthous, M. Guebre-Xabier, B. Murrell, N. Patel, G. Glenn, G. Smith and K. Loré, *npj Vaccines*, 2024, **9**, 17.

13. Q. Zhang and X. Cao, *Nat Rev Immunol*, 2019, **19**, 417-432.

14. O. T. Ranzani, M. D. T. Hitchings, R. L. de Melo, G. V. A. de França, C. d. F. R. Fernandes, M. L. Lind, M. S. S. Torres, D. H. Tsuha, L. C. S. David, R. F. C. Said, M. Almiron, R. D. de Oliveira, D. A. T. Cummings, N. E. Dean, J. R. Andrews, A. I. Ko and J. Croda, *Nature Communications*, 2022, **13**, 5536.

15. N. Pardi and D. Weissman, *Nat Biomed Eng*, 2020, **4**, 1128-1133.

16. S. Lei, X. Chen, J. Wu, X. Duan and K. Men, *Signal Transduct Target Ther*, 2022, **7**, 387.

17. B. Cosar, Z. Y. Karagulleoglu, S. Unal, A. T. Ince, D. B. Uncuoglu, G. Tuncer, B. R. Kilinc, Y. E. Ozkan, H. C. Ozkoc, I. N. Demir, A. Eker, F. Karagoz, S. Y. Simsek, B. Yasar, M. Pala, A. Demir, I. N. Atak, A. H. Mendi, V. U. Bengi, G. Cengiz Seval,

E. Gunes Altuntas, P. Kilic and D. Demir-Dora, *Cytokine Growth Factor Rev*, 2022, **63**, 10-22.

18. P. Deb, M. M. A. Molla and K. M. Saif-Ur-Rahman, *Biosaf Health*, 2021, **3**, 87-91.

19. Y. M. Báez-Santos, S. E. St John and A. D. Mesecar, *Antiviral Res*, 2015, **115**, 21-38.

20. D. J. Calleja, G. Lessene and D. Komander, *Front Chem*, 2022, **10**, 876212.

21. C. B. McClain and N. Vabret, *Signal Transduction and Targeted Therapy*, 2020, **5**, 223.

22. M. Saramago, V. G. Costa, C. S. Souza, C. Bárria, S. Domingues, S. C. Viegas, D. Lousa, C. M. Soares, C. M. Arraiano and R. G. Matos, *Microorganisms*, 2022, **10**.

23. Y. Kim, J. Wower, N. Maltseva, C. Chang, R. Jedrzejczak, M. Wilamowski, S. Kang, V. Nicolaescu, G. Randall, K. Michalska and A. Joachimiak, *Communications Biology*, 2021, **4**, 193.

24. D. A. Jamison, S. Anand Narayanan, N. S. Trovão, J. W. Guarnieri, M. J. Topper, P. M. Moraes-Vieira, V. Zaksas, K. K. Singh, E. S. Wurtele and A. Beheshti, *European Journal of Human Genetics*, 2022, **30**, 889-898.

25. J. Chen, R. A. Farraj, D. Limonta, S. A. Tabatabaei Dakhili, E. M. Kerek, A. Bhattacharya, F. M. Reformat, O. M. Mabrouk, B. Brigant, T. A. Pfeifer, M. T. McDermott, J. R. Ussher, T. C. Hobman, J. N. M. Glover and B. P. Hubbard, *J Biol Chem*, 2023, **299**, 105341.

26. M. C. Pillon, M. N. Frazier, L. B. Dillard, J. G. Williams, S. Kocaman, J. M. Krahn, L. Perera, C. K. Hayne, J. Gordon, Z. D. Stewart, M. Sobhany, L. J. Deterding, A. L. Hsu, V. P. Dandey, M. J. Borgnia and R. E. Stanley, Nat Commun, 2021, 12, 636.

Chapter 2

Applied techniques

2.1 High throughput screening

High Throughput Screening (HTS) is a vital process in modern drug discovery, enabling the automated testing of thousands to millions of compounds against specific biological targets.[1] This method begins with creating a diverse chemical library, including small molecules, peptides, or biologics, which are then screened using miniaturized assays in microtiter plates with wells ranging from 96 to 1536. Automation is crucial in HTS, facilitating the rapid and precise handling of compounds, reagents, and biological samples. The screening assays can be either biochemical, measuring enzyme activity, or cell-based, assessing effects on living cells such as viability or signaling pathways. The data generated are analyzed using advanced software to identify promising compounds. HTS is celebrated for its speed, allowing vast libraries to be screened in days or weeks, significantly accelerating the drug development process compared to traditional methods. It is also cost-effective, conserving resources by eliminating less promising compounds early. HTS can reveal novel drug candidates and biological targets, aiding in lead optimization by refining initial hits for better efficacy and reduced toxicity. However, HTS faces challenges such as the risk of false positives and negatives, requiring robust assays and confirmatory testing.[2] The complexity of biological systems and the need for sophisticated informatics solutions to manage large datasets further complicate the process. Despite these challenges, HTS remains essential for target identification, lead optimization, and understanding drug mechanisms, making it a cornerstone of pharmaceutical research and development and promising an increasingly pivotal role in discovering effective treatments for various diseases.

Förster Resonance Energy Transfer (FRET)

Förster Resonance Energy Transfer (FRET) is a highly sensitive and versatile technique that has revolutionized the study of molecular interactions and dynamics at the nanoscale level.[3] FRET relies on the non-radiative transfer of energy between two fluorophores: a donor and an acceptor. When these fluorophores are in close proximity—typically

within 1-10 nanometers—the energy absorbed by the donor is transferred to the acceptor, resulting in fluorescence emission at a longer wavelength. This mechanism makes FRET an invaluable tool for investigating protein-protein interactions, conformational changes, and other molecular events within living cells. The technique's ability to provide real-time, quantitative measurements of interactions and conformational shifts with high spatial resolution is due to its reliance on the precise overlap of the emission spectrum of the donor and the absorption spectrum of the acceptor. The FRET assay is particularly advantageous for studying dynamic processes and interactions in their native cellular environments, offering insights into biological phenomena that traditional methods might miss. By employing various fluorophore pairs and assay formats, researchers can tailor FRET assays to specific experimental needs, enhancing their ability to probe complex molecular mechanisms. Despite its powerful capabilities, FRET requires careful optimization of fluorophore selection, assay conditions, and data interpretation to overcome challenges such as background noise and signal interference. Nonetheless, the FRET assay continues to be a cornerstone of modern molecular and cellular research, driving advancements in drug discovery, functional genomics, and cell biology through its ability to reveal intricate details of molecular interactions and cellular processes with unprecedented clarity.

Activity-Based Protein Profiling (ABPP) assay

Activity-based protein profiling (ABPP) is a transformative approach in drug discovery that focuses on assessing the functional activity of proteins within complex biological systems.[4] Unlike traditional proteomics methods that primarily quantify protein abundance, ABPP enables researchers to understand the active states of proteins, particularly enzymes, and how they interact with potential therapeutic agents. This innovative technique has garnered significant attention for its potential to enhance target identification, elucidate drug mechanisms, and streamline the development of novel therapeutics.

ABPP utilizes small-molecule probes that covalently bind to the active sites of target proteins to provide detailed insights into their function. These probes are composed of a reactive group that interacts specifically with the enzyme's active site and a detectable tag, such as a fluorophore or biotin.[5] The ABPP process begins with the design and synthesis of these probes, which must be tailored to selectively label proteins based on their catalytic mechanisms or functional groups. The biological sample, whether cell lysates or tissue extracts, is then treated with the probe, allowing it to form stable covalent bonds with active proteins. Following labeling, the modified proteins are isolated through methods like affinity purification, and their presence is detected using techniques such as mass spectrometry, western blotting, or fluorescence-based assays. Finally, the labeled proteins undergo functional analysis to elucidate their roles in biological pathways, interactions with other molecules, and responses to drugs, thereby advancing drug discovery efforts and enhancing our understanding of protein functions.

ABPP presents several notable advantages over traditional drug discovery methodologies. It focuses on the functional activity of proteins rather than merely their presence,

offering deeper insights into their roles in disease states and enabling more informed target selection. ABPP is particularly effective in identifying active enzymes that may serve as novel drug targets, uncovering therapeutic avenues that might otherwise be overlooked. The selective labeling capability of ABPP probes enhances the sensitivity and accuracy of target identification within complex biological mixtures, which is crucial for working with heterogeneous samples. Additionally, ABPP provides mechanistic insights into drug candidates, revealing how these compounds interact with their targets and aiding in the optimization of lead compounds. In drug discovery applications, ABPP is widely used for enzyme target identification, helping to characterize enzymes involved in diseases like cancer and infectious diseases. It also elucidates drug mechanisms by analyzing interactions with protein active sites, leading to improved drug design. Furthermore, ABPP can uncover allosteric modulators, which may offer benefits such as enhanced selectivity and reduced side effects compared to traditional inhibitors. Additionally, ABPP contributes to biomarker discovery by identifying active protein signatures associated with specific diseases, thereby improving patient stratification in clinical trials and enhancing therapeutic outcomes.

2.2 Cellular assays

cytotoxicity assay

The resazurin-based Cytotoxicity assay is a powerful tool for assessing cell viability in the context of evaluating the effects of endonuclease inhibitors, particularly in drug development.[6] This assay relies on the principle that resazurin, a blue dye that is non-toxic and permeates cell membranes, is reduced to resofurin, a pink, highly fluorescent compound, by metabolically active cells. This reduction is mediated by the cellular reducing agents, primarily in the mitochondria, making the assay a direct measure of cell metabolic activity and thus cell viability. In practice, cultured cells are exposed to various concentrations of endonuclease inhibitors, such as those targeting specific viral, to evaluate their cytotoxic effects. After an incubation period, resazurin is introduced to the cell culture medium. As viable cells metabolize the dye, it is converted to resofurin, and the fluorescence intensity is measured using a fluorescence microplate reader. The level of fluorescence is proportional to the number of living cells; hence, a decrease in fluorescence indicates the cytotoxic effects of the inhibitors. By analyzing the fluorescence data, researchers can determine the IC50 value, which represents the concentration of the inhibitor required to reduce cell viability by 50%. This provides crucial information about the potency and safety of the inhibitors. The resazurin assay is favored for its simplicity, sensitivity, and quantitative nature, allowing for precise evaluation of cellular health. Additionally, it is non-destructive, enabling ongoing observation of the same cell cultures over time. However, it is important to acknowledge its limitations. The assay's reliance on cellular metabolic activity means that it may not fully capture all aspects of cytotoxicity, particularly if the inhibitors affect cellular processes not directly linked to metabolism. Moreover, interference from certain compounds or cellular conditions can affect

the accuracy of the results. Despite these limitations, the resazurin assay remains a valuable approach for assessing the viability of cells treated with endonuclease inhibitors, providing essential data that informs the development of effective antiviral therapies and contributes to the broader effort to combat viral infections.

2.3 Molecular dynamics

Molecular dynamics (MD) simulations play a crucial role in the drug delivery field, particularly when evaluating inhibitors targeting endonucleases.[7] This computational technique provides a detailed and dynamic view of the interactions between small molecule inhibitors and their target proteins, such as endonucleases, which are often implicated in viral replication and other pathological processes. In the context of drug delivery, MD simulations offer insights into how inhibitors bind to endonucleases at the atomic level, revealing crucial information about binding affinity, stability, and the conformational changes that occur upon inhibitor binding. By simulating the interactions between inhibitors and endonucleases over time, researchers can observe how inhibitors engage with specific amino acid residues within the enzyme's active site and how these interactions influence the enzyme's overall structure and function. This helps in understanding the mechanism of inhibition and in optimizing the chemical properties of the inhibitors for improved efficacy. Furthermore, MD simulations can predict how inhibitors behave in complex biological environments, such as within cellular membranes or in the presence of other biomolecules, providing valuable insights into their potential pharmacokinetics and pharmacodynamics. This information is essential for designing effective drug delivery systems that ensure targeted and efficient delivery of inhibitors to their intended site of action while minimizing off-target effects and improving therapeutic outcomes. However, the accuracy of MD simulations depends on the quality of the force fields used and the precision of the initial structural models, highlighting the need for high-quality data and advanced computational techniques. Overall, molecular dynamics simulations are an indispensable tool in the drug delivery field, offering a deep understanding of inhibitor-enzyme interactions and guiding the development of more effective and targeted therapies for conditions where endonucleases are key therapeutic targets.

Molecular docking

Molecular docking is a pivotal computational technique in drug discovery, especially when investigating the binding of inhibitors to endonucleases.[8] This method simulates the interaction between a small molecule inhibitor and a target enzyme, such as an endonuclease, to predict how well the inhibitor binds to the enzyme's active site and to assess the potential efficacy of the inhibitor. During the docking process, the three-dimensional structures of both the inhibitor and the endonuclease are used to explore various conformations and orientations of the inhibitor within the enzyme's binding site. The docking algorithm calculates the binding affinity by evaluating how well the inhibitor fits into the enzyme's active site

and how many favorable interactions, such as hydrogen bonds, hydrophobic interactions, and electrostatic forces, are formed. This interaction is quantitatively scored to predict the strength of the binding, providing insights into the inhibitor's potential effectiveness. Molecular docking helps in identifying key residues involved in binding and elucidating the mechanism of inhibition. For endonucleases, which play crucial roles in processes like viral replication and RNA processing, accurately predicting how an inhibitor binds can guide the design of more effective compounds that target specific active site residues or allosteric sites. Moreover, docking results can be used to refine inhibitor structures through iterative design, enhancing their binding affinity and specificity. By integrating docking results with experimental data, such as from X-ray crystallography or NMR spectroscopy, researchers can validate and optimize their drug candidates. Despite its power, molecular docking does have limitations, including dependence on the accuracy of the protein and ligand structures and the algorithms used to predict binding modes. Nonetheless, molecular docking remains a vital tool in drug discovery, providing essential insights into how inhibitors interact with endonucleases and aiding in the development of targeted therapies that can effectively disrupt enzyme function and treat various diseases.

2.4 References

1. M. Entzeroth, H. Flotow and P. Condron, *Curr Protoc Pharmacol*, 2009, **Chapter 9**, Unit 9.4.

2. R. Roy, S. K. Singh and S. Misra, *Challenges and the Advancement in High-Throughput Screening Strategies for Cancer Therapeutics*, 2023.

3. Y. Ueda, S. Kwok and Y. Hayashi, *Front Neural Circuits*, 2013, **7**, 163.

4. L. A. R. Carvalho and G. J. L. Bernardes, *ChemMedChem*, 2022, **17**, e202200174.

5. B. P. Kok, S. Ghimire, W. Kim, S. Chatterjee, T. Johns, S. Kitamura, J. Eberhardt, D. Ogasawara, J. Xu, A. Sukiasyan, S. M. Kim, C. Godio, J. M. Bittencourt, M. Cameron, A. Galmozzi, S. Forli, D. W. Wolan, B. F. Cravatt, D. L. Boger and E. Saez, *Nat Chem Biol*, 2020, **16**, 997-1005.

6. T. L. Riss, R. A. Moravec, A. L. Niles, S. Duellman, H. A. Benink, T. J. Worzella and L. Minor, in *Assay Guidance Manual*, eds. S. Markossian, A. Grossman, M. Arkin, D. Auld, C. Austin, J. Baell, K. Brimacombe, T. D. Y. Chung, N. P. Coussens, J. L. Dahlin, V. Devanarayan, T. L. Foley, M. Glicksman, K. Gorshkov, J. V. Haas, M. D. Hall, S. Hoare, J. Inglese, P. W. Iversen, M. Lal-Nag, Z. Li, J. R. Manro, J. McGee, O. McManus, M. Pearson, T. Riss, P. Saradjian, G. S. Sittampalam, M. Tarselli, O. J. Trask, Jr., J. R. Weidner, M. J. Wildey, K. Wilson, M. Xia and X. Xu, Eli Lilly & Company and the National Center for Advancing Translational Sciences, Bethesda (MD), 2004.

7. M. De Vivo, M. Masetti, G. Bottegoni and A. Cavalli, *J Med Chem*, 2016, **59**, 4035-4061.

8. X. Y. Meng, H. X. Zhang, M. Mezei and M. Cui, *Curr Comput Aided Drug Des*, 2011, **7**, 146-157.

Chapter 3

Discovery of a covalent inhibitor against Papain-like protease (PLpro) from SARS-CoV-2 (SCoV-2)

3.1 Abstract

The papain-like protease (PLpro) plays a critical role in SARS-CoV-2 (SCoV-2) pathogenesis and is essential for viral replication and for allowing the virus to evade the host immune response. Inhibitors of PLpro have great therapeutic potential, however, developing them has been challenging due to PLpro's restricted substrate binding pocket. In this report, we screened a 115,000-compound library for PLpro inhibitors and identified a new pharmacophore, based on a mercapto-pyrimidine fragment that is a reversible covalent inhibitor (RCI) of PLpro and inhibits viral replication in cells. Compound 5 had an IC_50 of 5.1 μM for PLpro inhibition and hit optimization yielded a derivative with increased potency (IC_50 0.85 μM, 6-fold higher). Activity based profiling of compound 5 demonstrated that it reacts with PLpro cysteines. We show here that compound 5 represents a new class of RCIs, which undergo an addition elimination reaction with cysteines in their target proteins. We further show that their reversibility is catalyzed by exogenous thiols and is dependent on the size of the incoming thiol. In contrast, traditional RCIs are all based upon the Michael addition reaction mechanism and their reversibility is base-catalyzed. We identify a new class of RCIs that introduces a more reactive warhead with a pronounced selectivity profile based on thiol ligand size. This could allow the expansion of RCI modality use towards a larger group of proteins important for human disease.

3.2 Introduction

The severe acute respiratory syndrome coronavirus 2 (SCoV-2) has caused catastrophic levels of death and effective treatments are urgently needed.[1–4] Small molecule therapeutics that

can inhibit the RNA dependent polymerase (RdRp) and Main protease (Mpro) are clinically approved and had a big impact on reducing COVID-19 mortality.[5–8] The success of these small molecule drugs has created a tremendous interest in developing inhibitors against other proteins from SCoV-2 that are also essential for viral replication.[9,10]

The papain-like protease (PLpro) from SCoV-2 is an essential protein for viral replication and an attractive target for developing small-molecule drugs.[11–14] PLpro plays a crucial role in viral replication[15–17] and prevents infected cells from generating interferons, which are essential for mounting an immune response against SCoV-2.[12,18,19] PLpro cleaves the peptide sequence LxGG (x represents any amino acid), which is present in 3 sites in the immature SCoV-2 viral polyprotein. PLpro catalyzes the release of three non-structural proteins, termed nsp1, nsp2, and nsp3 from the immature viral polyprotein.[12] Nsp1, nsp2, and nsp3 play critical roles in viral replication, and inhibition of PLpro blocks SCoV-2 replication in cells.[2]0 PLpro also cleaves host proteins that contain the sequence RLRGG, which is present in several ubiquitin (Ub) and ubiquitin-like proteins (UbL), such as interferon-induced gene 15 (ISG15) proteins.[21] PLpro has significant deISGylating and deubiquitinating activities and inhibition of PLpro induces the production of interferons by virally infected cells, which should lead to an enhanced immune response against the virus. Consequently, there is great interest in developing inhibitors against PLpro from SCoV-2.
textsuperscript14,20

PLpro is a cysteine protease with a catalytic triad composed of histidine, cysteine, and aspartic acid, with 83% sequence homology to PLpro from SCoV and structural similarities to the deubiquitinating enzymes.[12] Several crystal structures of PLpro have been solved,[22] and these studies have revealed that it binds Gly–Gly in the first two positions of its peptide binding site, and does not have a well-defined binding pocket near its active site, in contrast to other proteases that need to accommodate peptides with larger side chains.[23] PLpro is a challenging protein to drug due to its ill-defined binding pocket, and progress towards developing PLpro inhibitors has been slow despite its great antiviral potential.[3,20,24,25]

Several high throughput screens (HTS) have been performed against PLpro from SCoV and SCoV-2, and these studies have generated pharmacophores that can inhibit PLpro and viral replication in cells [26, 27]. The compound GRL0617 and its derivatives are the best characterized class of PLpro inhibitors. GRL0617 was identified in a 50,080-molecule screen on PLpro from SCoV [28]. GRL0617 inhibited SCoV PLpro with an IC_{50} in the low micromolar range and can inhibit viral replication in cells. GRL0617 also inhibits PLpro from SCoV-2 and viral replication in cells, with IC_{50}s in the micromolar range, and shows moderate antiviral activity against SCoV-2 in mice after oral delivery [11, 22, 25-27, 29]. GRL0617 has been further optimized against PLpro from SCoV-2, via structure-based drug design strategies, and its derivatives inhibit PLpro with nanomolar efficacy *in vitro* and inhibit viral replication in cells efficiently [22-24, 26, 27, 30, 31].

Additional HTS screens on PLpro from SCoV-2 have generated other non-GRL0617 based pharmacophores that are promising leads [26, 32]. For example, Yuan et al. screened a 50,080 large compound library and identified a new class of PLpro inhibitors, based upon the fragment 5-oxo-1-thioxo-4,5-dihydro[1,3] thiazolo[3,4-a]quinazoline-3- carboxamide, which was

able to inhibit PLpro from multiple corona viruses and inhibited SCoV-2 viral replication in hamsters and MERS-CoV in mice, and outperformed GRL0617 in animal studies [33]. These experiments demonstrate the great potential of non-GRL0617 based chemical scaffolds. There are currently very few non-GRL0617 based scaffolds that can inhibit PLpro and viral replication in cells [20, 32] and alternatives to GRL0617 and its derivatives are greatly needed, given the high failure rate of small molecule therapeutics in clinical trials.

In this report, we screened a 115,000-molecule chemical library against PLpro from SCoV-2 and discovered a unique mercaptopyrimidine based pharmacophore, compound 5, which inhibits PLpro in vitro and inhibits SCoV-2 viral replication in cells. In addition to compound 5, we also identified several other compounds that were able to inhibit PLpro, which could serve as leads for further optimization. Finally, the mechanism by which compound 5 inhibits PLpro was also investigated by activity-based profiling, molecular dynamics, and a variety of other biochemical assays.

3.3 Results and discussion

Discovery of compounds inhibiting PLpro via high throughput screening

We used a fluorescent-based high throughput screening assay to identify inhibitors for PLpro from SCoV-2.[28] This fluorescent assay uses RLRGG-AMC as a substrate for determining PLpro proteolytic activity. The release of the AMC was quantified by measuring the fluorescent intensity after exciting at 360 nm and measuring the emission at 460 nm. The PLpro domain of Nsp3 was recombinantly expressed and purified using a talon column. We optimized the protein and substrate concentration to 50 nM and 50 μM respectively, and our optimized assay had a z' factor of 0.57 $\pm$ 0.05, suitable for HTS. We screened two libraries, termed the diverse and antibacterial libraries (115,000 compounds) at the concentration of 40 μM, and compounds that generated ¿50% inhibition were rescreened in duplicate, followed by a dose–response assay to determine the concentration that caused 50% PLpro inhibition (IC_{50}) (Fig. 3.1).

The preliminary screening of the diverse and antibacterial libraries resulted in 560 initial hits at a 3-sigma cutoff, and our screen had a hit rate of 0.48%. We further performed orthogonal assays to ensure that positive hits were not interacting directly with the fluorescence of the released coumarin-amine, reducing the hits to 211. A dose-response experiment was performed to determine the half maximal inhibitory concentration of the top 84 hits which revealed that ten compounds out of 115,000 were capable of inhibiting PLpro from SCoV-2 *in vitro* with IC_{50} less than 10 µM (Figure 1B). Several of the remaining hits were electrophiles and some were unique from inhibitors reported in previous articles. Four out of the ten compounds, compounds 2, 6, 7, and 10 share the same parent heterocycle structure and electrophilic warhead as the compound recently reported by Yuan et al. [33], which showed antiviral activity in cells and in animals, and this pharmacophore has great potential

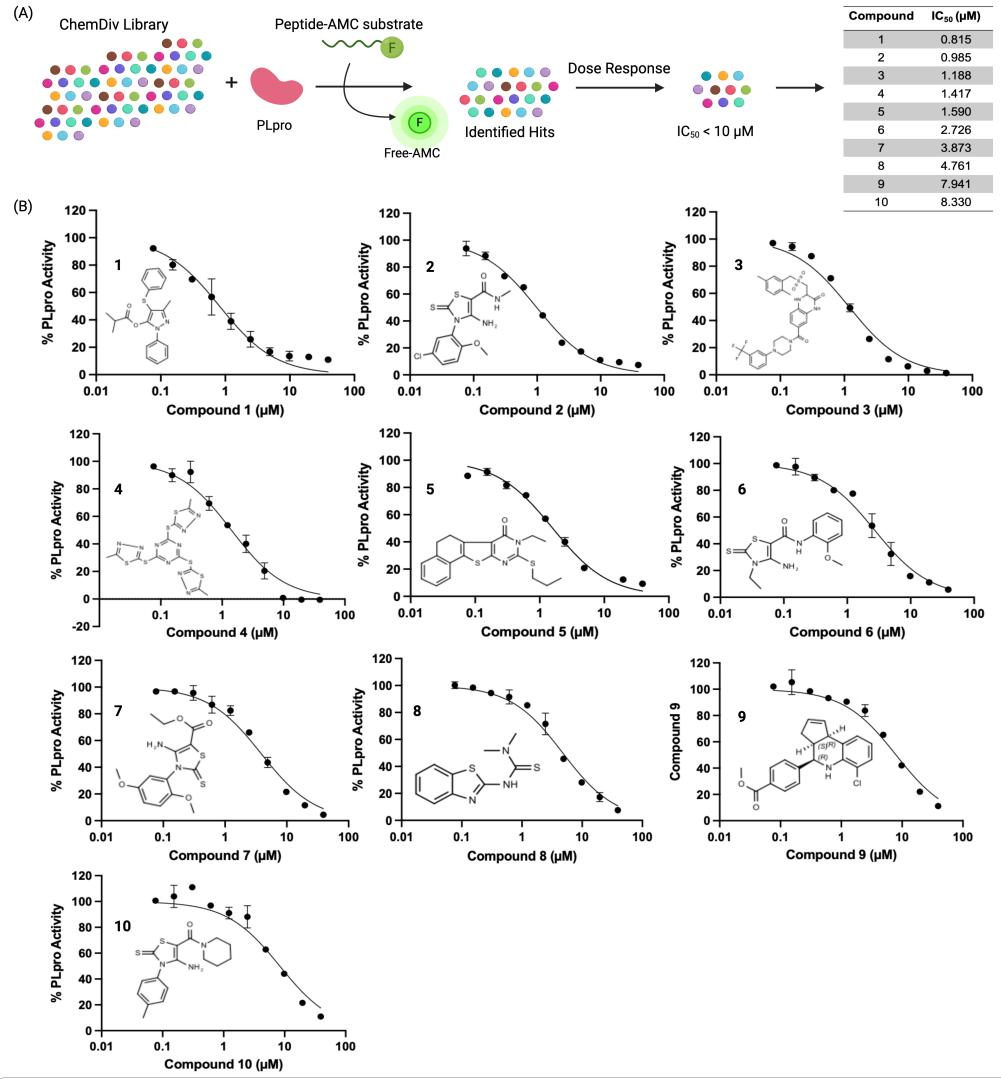

Compound	IC_{50} (μM)
1	0.815
2	0.985
3	1.188
4	1.417
5	1.590
6	2.726
7	3.873
8	4.761
9	7.941
10	8.330

Figure 3.1: High throughput screening of a 115,000-compound library against PLpro identifies inhibitors with sub-micromolar IC_{50}s.

for further exploration. In addition, all of the compounds (1-10) are alkaloids, which have shown great potential as SCoV-2 antiviral agents[34].

Compound 5 exhibits anti-SCoV-2 activity

To test antiviral activity, the top hits were screened on nano luciferase (NLuc) SCoV-2 infected TMRPSS2-expressing Vero E6 cells at various concentrations (1, 10, or 20 μM). Of the compounds tested, one compound exhibited antiviral activity in a dose dependent manner. Compound 5 reduced the NLuc levels of infected cells by 3-fold at 10 μM and 7-fold at 20 μM (Fig. 3.2A). To validate the antiviral activity of compound 5, a separate antiviral study was performed with compound 5 using a plaque forming assay. The viral plaque forming assay validated the antiviral activity of compound 5 and compound 5 caused a 3 and 22-fold reduction in infectious virus levels at 10 μM and 20 μM concentrations, respectively. Remdesivir (100 μM) served as a positive control in this assay and potently inhibited the virus (Fig. 3.2B). Finally, to ensure that the antiviral activity of compound 5 was not due to cytotoxicity, we performed a cell viability assay using the resazurin assay. Compound 5 was tested at four concentrations (1, 10, 25, 50 μM) in Vero CCL-81 cells and the cell viability at 1, 10 and 25 μM of compound 5 was greater than 85%. However, compound 5 had significant toxicity at a 50 μM concentration (Fig. 3.2C).

Compound 5 is a covalent PLpro inhibitor

Compound 5 contains a mercaptopyrimidine fragment, which can potentially undergo addition–elimination reactions with nucleophiles. For example, Murugesan et al. recently identified a mercaptopyrimidine based inhibitor of tuberculosis cell growth, which reacted with glutathione under physiological conditions.[27,35] PLpro is a cysteine protease with a nucleophilic cysteine in its active site, which could potentially react with compound 5*via* an additional elimination reaction. We performed a time dependent PLpro inhibition assay with compound 5 to determine if pre-incubation time lowered its IC_{50}. Pre-incubation time lowers the IC_{50} of covalent inhibitors because it gives more time for the protein to react with the inhibitor. In contrast, pre-incubation time frequently has no effect on the IC_{50} of non-covalent inhibitors because their k_{offs} are generally on the timescale of second to minutes. PLpro was preincubated with compound 5 for various times ranging from 5 minutes to 3 hours and the IC_{50} of compound 5 was measured for each pre-incubation time point. The IC_{50} of compound 5 decreased by 10-fold after pre-incubation with PLpro for 3 hours (Fig. 3.3A), suggesting it is a covalent inhibitor.

We performed activity-based profiling experiments to determine if compound 5 covalently reacted with the cysteines or lysines of PLpro.[36] Iodoacetamide-rhodamine was used as the probe for cysteine reactivity analysis and NHS-rhodamine was the probe for investigating lysine reactivity on PLpro. A traditional pulse chase experiment was performed with PLpro and the rhodamine dyes, where PLpro was first incubated with compound 5 and then incubated with iodoacetamide-rhodamine or NHS-rhodamine. After the dye incubation, PLpro

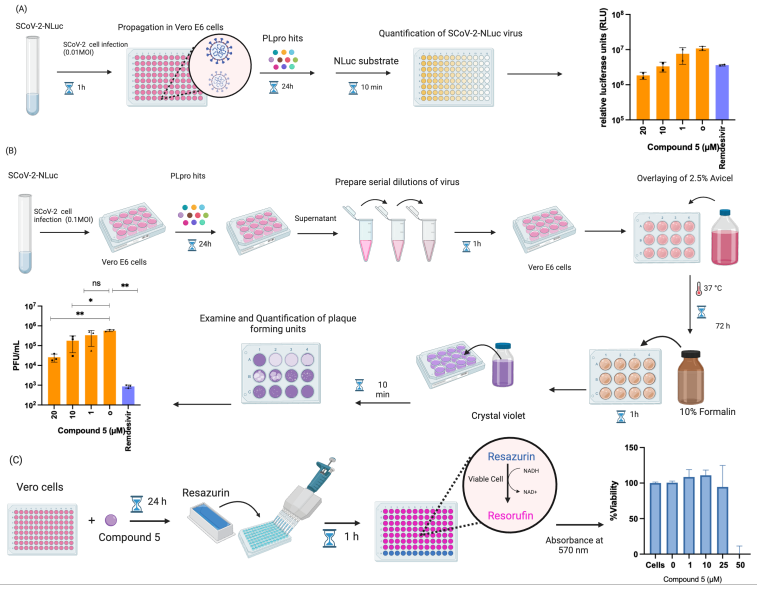

Figure 3.2: Compound 5 inhibits SCoV-2 replication in cells. Cytotoxicity assay of compound 5.

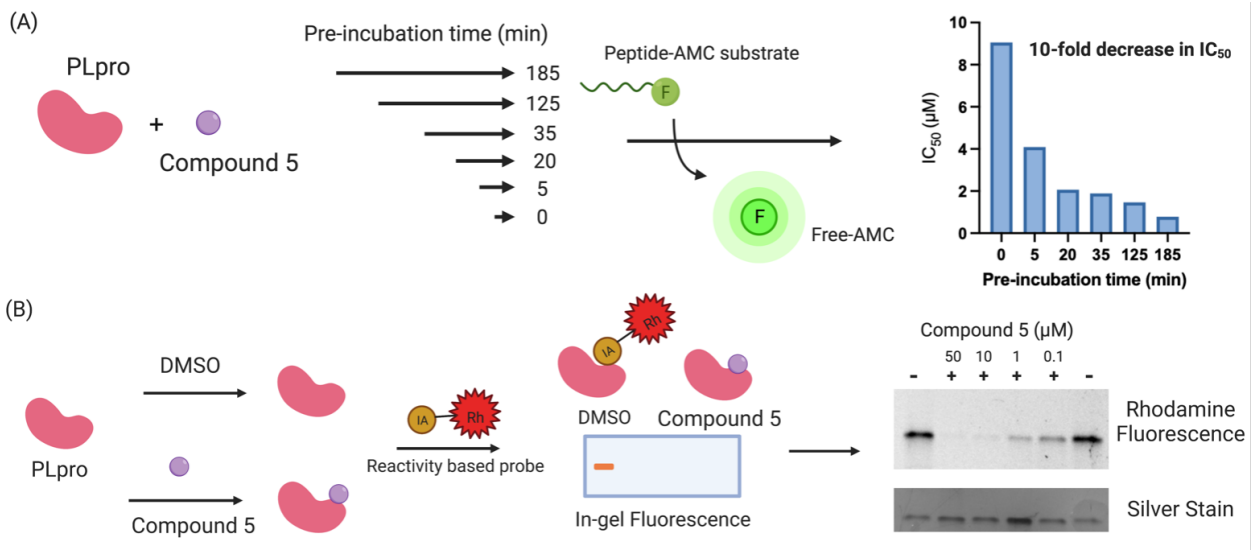

Figure 3.3: Compound 5 is a covalent inhibitor of PLpro.

was run on a protein gel and imaged via fluorescence. Compound 5 was able to prevent PLpro from reacting with iodo-acetamide, demonstrating that it reacts with nucleophilic thiols on PLpro, most likely the catalytic cysteine in the active site (Fig. 3.3B). The other thiols in PLpro are either disulfides, which are unreactive to nucleophiles, or zinc chelated and have diminished nucleophilicity. In contrast to iodoacetamide, compound 5 was unable to prevent PLpro from reacting with NHS-rhodamine, demonstrating that it is not reacting with lysine residues.

Compound 5 is a reversible covalent inhibitor of PLpro

Compound 5 contains a mercaptopyrimidine fragment, which can potentially react with PLpro in a reversible manner *via* the addition–elimination reaction pathway. Reversible covalent inhibitors (RCIs) have great potential as electrophilic warheads because they combine the high efficacy of covalent inhibitors with the low toxicity of non-covalent inhibitors.[37] In addition, RCIs are less immunogenic than covalent inhibitors and their on-target residence time and therapeutic effectiveness can be fine-tuned by modulating their binding affinity with the target protein.38 However, developing RCIs is challenging because there are very few electrophiles that reversibly react with biological nucleophiles under physiologic conditions. At present, Michael addition acceptors are the only class of electrophilic warheads that can generate RCIs, and this limits the development of RCIs because numerous proteins do not react with the relatively mild/inert Michael acceptors. Compound 5 does not contain a Michael acceptor but has the potential to be an RCI because of the relatively low pKa of the thiol fragment attached to the pyrimidine ring, which could potentially be displaced by an incoming nucleophile.

To investigate if compound 5 constitutes a novel class of RCI, we performed a jump dilution assay with PLpro, compound 5 and beta-mercaptoethanol (BMe). PLpro and compound 5 were mixed and allowed to react, diluted 25-fold in the presence of 5 mM BMe [38], [39] and the inhibition of PLpro was measured. We observed that PLpro recovered 90% of its activity after 5 minutes dilution with 5 mM BMe (Fig. 3.4A), in contrast dilution in phosphate buffer saline (PBS) had no effect on the activity of PLpro. BMe is not a biological nucleophile, and we re-did the jump dilution assay in the presence of either 5 mM reduced glutathione (GSH) or 200 μM cysteine (their physiological concentrations)[40] to determine if the PLpro-compound 5 adduct would rapidly decompose in cells. We observed that the addition of cysteine recovered the activity of PLpro, however GSH did not (Fig. 3.4B). These experiments suggest that compound 5 is an RCI and its reversibility is based upon the size of the displacing thiol. Glutathione is larger than cysteine and BMe and presumably cannot access the active site of PLpro and therefore does not displace compound 5 from PLpro. In contrast, smaller thiols such as BMe and cysteine can apparently access the PLpro active site and can displace compound 5. Collectively, these experiments demonstrate compound 5 is an RCI and that the mercaptopryimidine ring can act as a new scaffold for generating RCIs that are not based upon Michael addition reactions. In addition, the mercaptopryimidine

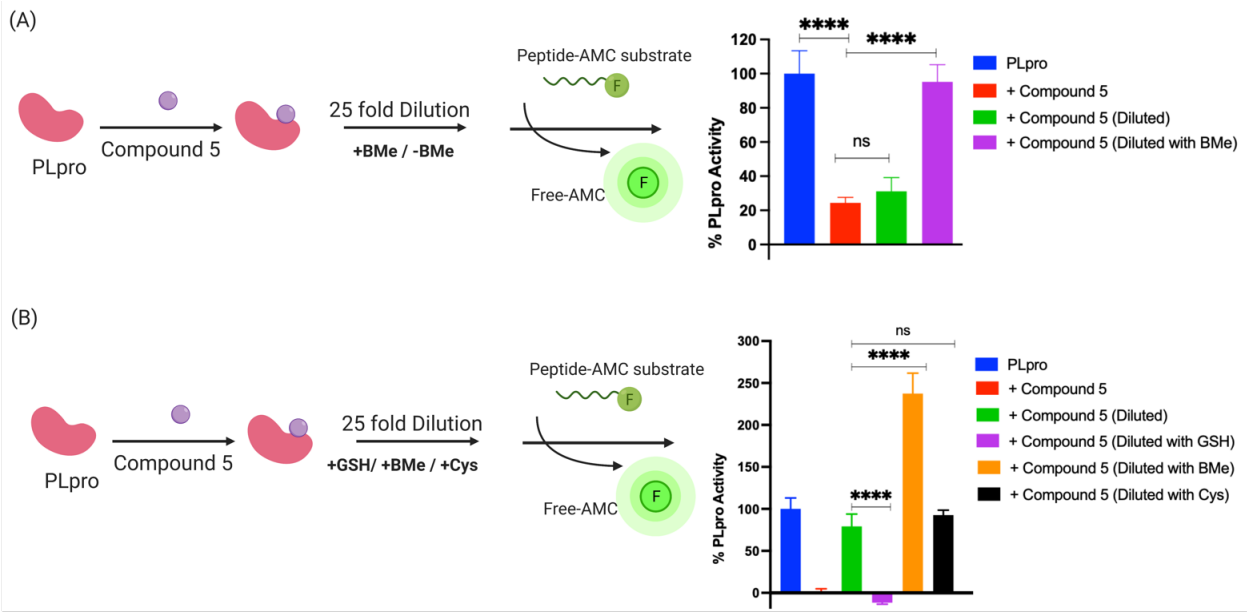

Figure 3.4: Compound 5 is a reversible covalent inhibitor of PLpro and its reversibility is triggered by exogenous thiols.

ring can function as a size selective filter for thiols and this unique feature should allow it to find numerous applications in drug discovery.

Compound 5 tolerates modifications of its mercapto group

We performed a preliminary hit exploration of compound 5 derivatives to identify sites in compound 5 that could be modified to enhance its activity. Compound 5 derivatives with modifications at site I, site II and site III were investigated for their ability to inhibit PLpro activity (Fig. 3.5A). Compound 5 does not tolerate modifications at site I and site II, and these derivatives were largely inactive. In contrast, modifications at site III were tolerated and resulted in several derivatives that were more active than compound 5 (Fig. 3.5B). For example, compound 5E contained an allylic thiol instead of a propyl thiol and had an IC_{50} of 0.9 μM, which was approximately 5 times lower than compound 5. In addition, compound 5B, which had an ethyl substituent on the thiol was also tolerated and had an IC_{50} of 5.0 μM and was almost identical to compound 5 (Fig. 3.5C). Substituents larger than a propyl group on the thiol, such as butyl, were not tolerated and resulted in almost a complete loss of activity. Although compounds 5B and 5E acted as PLpro inhibitors, they did not have any antiviral activity in Vero E6 cells as determined by a plaque assay (Fig. 3.6B).

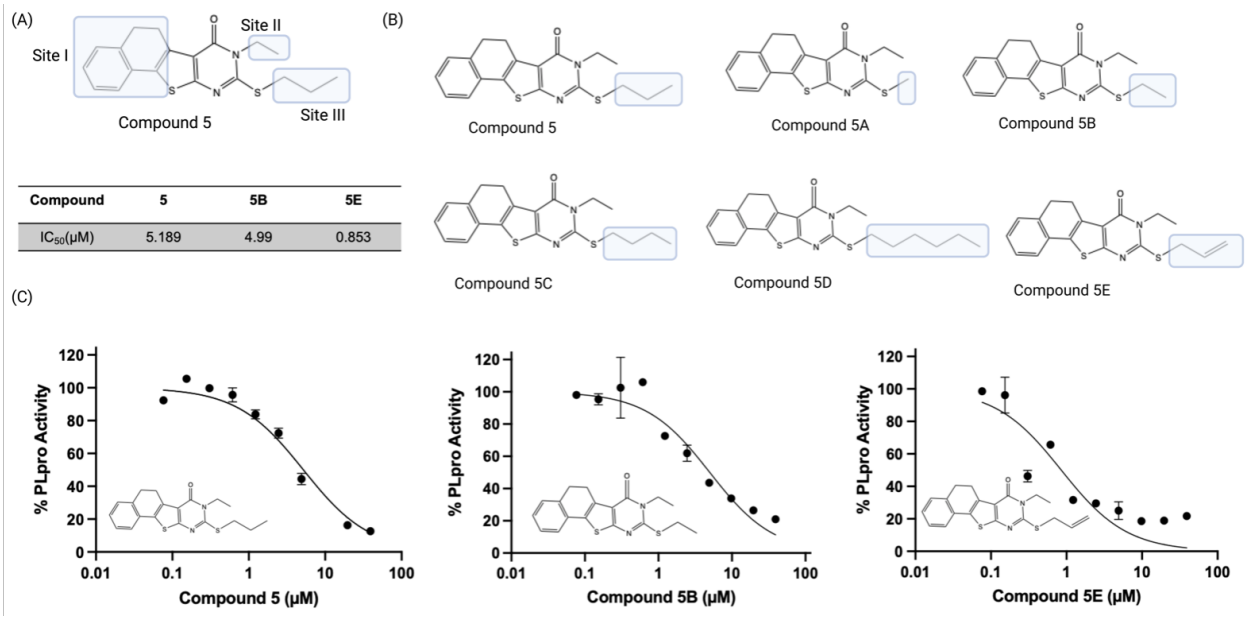

Figure 3.5: SAR of Compound 5 demonstrates it that tolerates modification at its mercapto group.

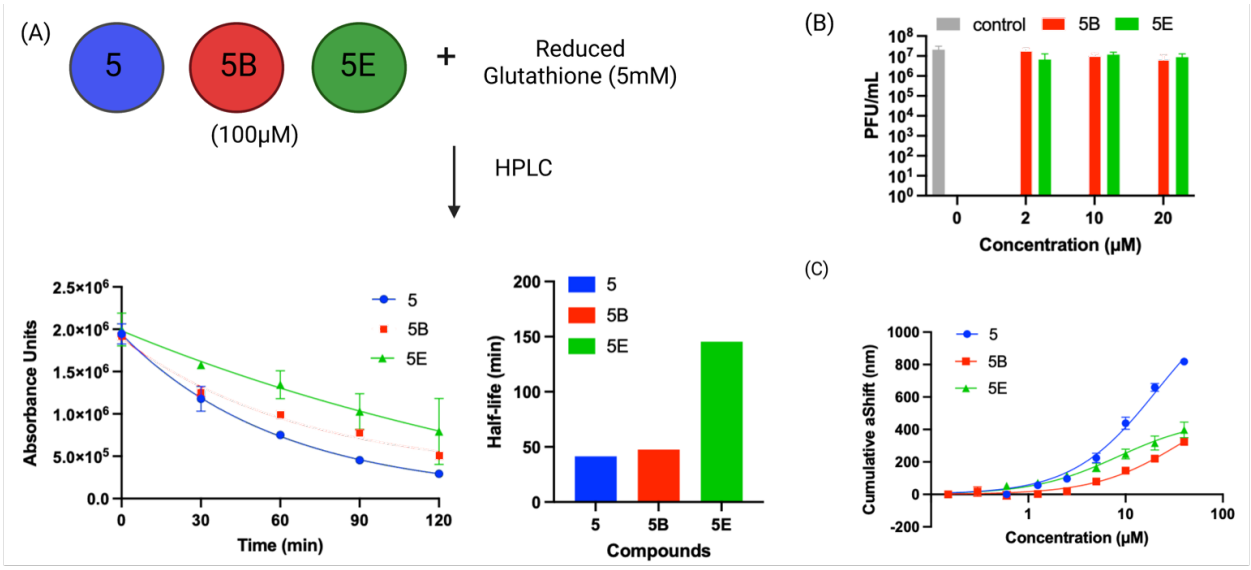

Figure 3.6: Compound 5 has low reactivity with thiols and binds PLpro with micromolar affinity.

Compound 5 has low non-specific reactivity with thiols

Compound 5 and the mercaptopyrimidine fragment represent a new under-explored class of electrophiles with numerous potential applications given their biological activity. The thiol reactivity of mercaptopyrimidines under physiologic conditions has never been investigated. We determined the half-life of compound 5 and its derivatives in the presence of 5 mM GSH via HPLC to gauge its reactivity in comparison to other electrophiles commonly used in generating covalent inhibitors. The GSH half-lifes of compounds 5, 5B and 5E varied between 41.0 minutes to 145.4 minutes (Fig. 3.6A) and are in a similar range to phenyl acrylamide-based electrophiles ($t\frac{1}{2}$ of 179 minutes with 5 mM GSH) which are a commonly used scaffold for generating covalent inhibitors [41]. For example, the clinically approved covalent kinase inhibitors afatinib, neratinib and osimertinib are all based upon phenyl acrylamide-based electrophiles.

Surface plasmon resonance (SPR) analysis of compound 5 and its derivatives

We performed SPR analysis of compound 5 and its derivatives with PLpro to determine their binding affinity with PLpro. His-tagged PLpro was immobilized on Ni-NTA sensor chips and various concentrations of compound 5 and its analogs (5B and 5E) were applied to the chip and the plasmon responses were recorded. The SPR results obtained with compound 5 and its analogs demonstrate that these compounds can bind PLpro and their binding affinity correlates with their IC_{50}s. For example, 5E had an inhibition IC_{50} of 0.85 μM and had a K_D of 8.3 μM, and compound 5 had an IC_{50} of 5.0 μM and had a K_D of 21 μM(Fig. 3.6C). The allyl modification of 5E is the only difference between compounds 5 and 5E and appears to significantly enhance 5E's interaction with PLpro.

Molecular dynamics simulation of compound 5 with PLpro

We performed a molecular dynamics simulation of compound 5 with the active site of PLpro to obtain insight into the potential interactions it may have with the active site. Compound 5 was covalently tethered to the active site cysteine of PLpro and an MD simulation was run, three independent times for 90 ns each. After a few picoseconds of simulation all three simulations generated structures that had compound 5 turned towards Trp106 and it interacted with Trp106 *via* π–π stacking for most of each simulation (Fig. 3.7).

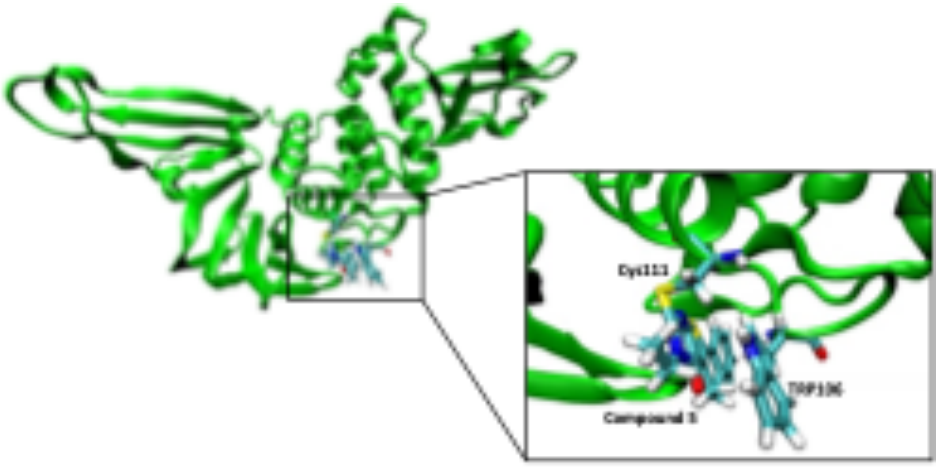

Figure 3.7: Molecular dynamic studies of Compound 5 with PLpro.

3.4 Experimental

Materials and methods

Expression and purification of PLpro

The papain-like protease (PLpro) expressing plasmid, 2BT-nsp3-PLpro was a kind gift from Ott lab at Gladstone Institute, UCSF. The plasmid was transformed into the *E. coli* BL21 (DE3) and plated on an ampicillin-resistant LB agar plate. The next day, a colony was picked up for overnight culture in the presence of ampicillin 100 μg mL^{-1}. For large-scale protein purification, a 1 L culture of 2XYT media was grown using overnight culture (1:100) at 37 °C (210 rpm). The bacterial culture was grown to $OD_{600}\sim$ 0.8–1.0 and induced with 1 mM IPTG. The protein was expressed at 20 °C for overnight (18–20 hours). Bacterial culture was harvested at 4000g, and cell pellets were resuspended in 30 mL lysis buffer (25 mM Tris–HCl pH 8.0, 250 mM NaCl, 10% glycerol, 5 mM BMe), supplemented with protease inhibitor tablets (Pierce). The cell culture was sonicated at 20% amplitude for 7 minutes (0.5 s ON, 1.5 s OFF). Cellular debris was pelleted down by centrifuging at 15,000g for 20 minutes at 4 °C. Supernatant was loaded on Talon column (GE Healthcare Life Sciences) (pre-equilibrated with lysis buffer) at speed of 1 mL/min. Non-specific proteins were washed with 20 column volumes of buffer A (lysis buffer supplemented with 25 mM imidazole). PLpro protein was eluted with 5-column volumes of buffer-B (lysis buffer supplemented with 250 mM imidazole). The eluted protein was concentrated using 10 kDa MWCO filter (Amicon-Millipore) up to 2 mg mL^{1}.

Fluorescent assay to determine the activity of the proteins

The kinetic assays were developed in 384 well plates to optimize the assay conditions (protein and substrate concentration, and incubation times) as described in Ratia et al.28 In brief description, the assays were set up with different concentration of protein (0–100 nM), different concentration of substrate (0–200 μM) and the fluorescent emission intensity was measured at different time intervals (0–30 minutes). The final reaction volume of 50 μL consisted of 30 μL of buffer (20 mM Hepes pH 7.5, 100 mM NaCl, 0.1% mg mL^1 BSA), 10 μL of protein, and 10 μL substrate. The fluorogenic peptide substrate Arg-Leu-Arg-Gly-Gly-AMC (Z-RLRGG-AMC) (Bachem Biosciences) acted as reaction initiator and fluorescent emission intensity was measured at given wavelengths (excitation: 360 nm and emission: 460 nm) at time intervals.

High throughput screening

We developed a high throughput assay to screen a 115,000-compound library at UC Berkeley Drug Discovery Center (DDC) at the Center of Emerging and Neglected Diseases. The assay was optimized for 384 well black plates (corning 3573) with a total reaction volume of 25 μL, with equal volumes of protein and substrate (12.5 μL) and 0.5 μL of DMSO or compound (final concentration of 40 μM) dissolved in DMSO which was pre-plated with an Analytik-Jena Cybio liquid handler which was also used to add protein and substrate reagents later during the actual run. Protein and substrate were diluted in same buffer used in 4.2 with exception of Antifoam (Spectrum chemicals, Cat# A1302) with the ratio of 1:5000 that was added to reduce surface tension. The fluorescent emission intensity was measured at the intervals of 0, 10, 20, 30 and 60 minutes using a 2104 Envision reader (PerkinElmer; excitation: 360 nm and emission: 460 nm). The 60 minute time point yielded the best Z prime and was chosen as the end point for all screening. The data was analyzed using dose response curve models (4 parameter fit).

Hit confirmation and dose response

Hits from primary screen were cherry-picked on a Tecan Freedom EVO 150 for rescreening to confirm. Confirmation was done at 40 μM in duplicate and a 10 point 1:2 serial dilution for dose response starting at 40 μM was also run in duplicate. Along with the dose response assays, we performed an orthogonal assay to rule out false positives. The orthogonal assay included the substrate and compounds with buffer only (without protein).

Structure–activity relationship (SAR)

The compounds and analogs were purchased from ChemDiv. Both activity assays, fluorescent and dose response, were repeated with these compounds in two additional conditions, 0.01% Triton-X and 1 mM reduced glutathione (mimicking the cellular reducing conditions).

Cytotoxicity assay

Vero CCL-81 cells (provided by UC Berkeley Cell culture facility) were thawed at 37 °C and were grown in Dulbecco's Modified Eagle Medium (DMEM, high glucose and pyruvate) (Gibco) in 100 mm dish. The media was supplemented with 10% fetal bovine serum (FBS) and 1% antibiotic and antimycotic (100 U mL^{-1} penicillin and 100 μg mL^{-1} streptomycin). The cells were split into 96 well plate with the count of 10,000 cells per well. Each compound was added in well with different concentration (1, 10 and 20 μM) with the 0.5% of DMSO and incubated for 72 hours. After 72 hours, resazurin (10 μg mL^{-1}) was added and fluorescence intensity was measured at excitation: 560 nm and emission: 590 nm. The experiment was performed in triplicates.

Mammalian cell lines and culture conditions

Vero-E6 were procured from ATCC were cultured in DMEM (Corning) supplemented with 10% fetal bovine serum (FBS) (GeminiBio), 1% glutamine (Corning), and 1% penicillinstreptomycin (Corning) at 37 °C, 5% CO_2.

SCoV-2 virus culture

SCoV-2 isolate SCoV-2-NLuc and USA-WA1/2020 (BEI NR-52281) were used for all infection studies. The virus infection experiments were performed in a Biosafety Level 3 laboratory. Working stocks of SARS-CoV-2 were made in TMPRESS-2 expressing Vero-E6 cells and were stored at 80 °C until used.

Viral infection studies

SCoV-2 NLuc antiviral assay

Vero cells were seeded (12,000 cells per well) in a white opaque 96-well plate. After overnight incubation the cells were infected with SARS-CoV-2-NLuc at 0.01 multiplicity of infection (MOI). At 1 hour post infection (hpi) the working stock of the virus was replaced by multiple concentrations (20, 10 and 0.1 μM) of compounds. Remdesivir and DMSO were used as positive and negative controls respectively. At 24 hpi, 50 μL of Nano luciferase substrate (Promega) was added to each well and after 10 min of incubation at room temperature luciferase signals were measured using a Promega Glow Max microplate reader. The relative luciferase signal was recorded and plotted against compound concentration using software Prism.

SCoV-2 USA-WA1/2020 antiviral assay

Vero cells were seeded in a 12 well plate. After overnight incubation the cells were infected by SARS-CoV-2 USA-WA1/2020 strain at MOI of 0.1. The media was replaced by multiple concentrations (20, 10 and 0.1 μM) of compound B. Remdesivir and DMSO were used as

positive and negative controls respectively. The cells were further incubated at 37 °C and 5% CO_2 for 24 hours and culture supernatant were harvested for plaque assay.

Plaque-forming assays

Culture supernatants at 24 hpi were used for plaque assay. Vero cells were seeded (0.2 × 106 cells per well) in 12 well plates and after overnight incubation the cells were infected with differential concentrations of supernatants from test and control groups. After 1 h absorption period, the media in the wells was overlaid by 2.5% Avicel (Dupont, RC-591) and incubated for 72 hours. After incubation the Avicel was removed and cells were fixed in 10% formalin for one hour and stained with crystal violet for 10 minutes, for visualization of plaque forming units per ML.

Mechanism of inhibition

The PLpro protein (50 nM) was preincubated with different concentration of inhibitor (0, 1, 2.5, 5, 10 and 20 M) for different time points (0, 5, 10, 20, 35, 95, 125, 185 minutes). The substrate (50 M) was added and measured the fluorescence. The data was analyzed using Enzyme – inhibition, GraphPad Prism.

Half-life determination of compound 5 and its analogs

The half-life of compound 5 was determined using HPLC. 100 M of compound 5 and its analogs was incubated with 5 mM reduced glutathione at pH 7.4 for different time intervals (0, 30, 60, 90, 120 and 180 minutes). The positive control sample was run without reduced glutathione. The half-life was calculated using first-order reaction kinetic equation, $t1/2 = 0.693/k$.

Activity based protein profiling

For gel-based ABPP experiments with PLpro, pure SCoV2 PLpro protein (0.1 g per sample for IA-rhodamine and 0.05 g for NHS-rhodamine) was pretreated with either DMSO vehicle or desired dosage of compound 5 at 37 °C for 1 hour in 25 L PBS. Samples were subsequently treated with either 100 nM tetramethylrhodamine-5-iodoacetamide dihydroiodide (IA-rhodamine) (Setareh Biotech 6222) or 500 nM 5/6-carboxy-tetramethyl-rhoadmine succinimidyl ester (NHS-Rhodamine) (Thermo Scientific™ 46406) protected from light at room temperature for 1 hour. Samples were incubated with 10 L 4× Laemmli sample buffer, boiled at 95 °C for 10 min, and separated by SDS/PAGE. Probe-labeled proteins were analyzed by in-gel rhodamine fluorescence using a ChemiDoc MP (Bio-Rad). Protein loading was assessed by Silver Staining.

Jump dilution assay

PLpro was mixed with compound 5 at the 10-fold higher concentration of IC_{50} ($10 \times IC_{50}$) and allowed to form protein-inhibitor complex at saturating conditions at room temperature. The complex was then rapidly diluted in a buffer supplemented with 5 mM reduced glutathione, 5 mM beta-mercaptoethanol (BMe), 200 M cysteine to bring the compound's concentration of $1/10 \times IC_{50}$. After 5 minutes of dilution, the substrate was added and incubated for 30 minutes. The fluorescent intensities were read at the excitation wavelength of 360 nm and emission wavelength of 460 nm.

Molecular dynamic studies

To study molecular interactions between PLpro active site and the inhibitor, first we prepared chemical structure of covalent inhibitor by drawing it in MarvinSketch (ChemAxon 2019) and has been modified according to its final state after covalent bonding. For Molecular Dynamics (MD) simulation using GROMACS [42], we used CHARMMS36 [43] forcefield. So, to get the forcefield parameters of the inhibitor, we convert 2D structure into 3D using OpenBable [44] software and transferred them into CGENFF [43, 45-47] online server. Protein model of SARS-CoV-2 PLpro (PDB: 6W9C) was obtained from RCSB server. After preparing all forcefield parameters, we defined covalent inhibitor as a new residue by manually adding its parameters in the CHARMM36 residue definition file. Moreover, we needed to modify Cys111 of PLpro as well, to turn it into its final state after covalent bonding by changing its residue type from Cys to Cys2. Finally, we applied corresponding Sulfur-Carbon bond parameters by manually inserting them into the bonded forcefield parameters of CHARMM36.

After defining all parameters, the energy minimized inhibitor with 1-ClickDocking online server (https://mcule.com) is brought in vicinity of CYS111 using VMD [48]. The resulting protein complex were placed inside a water box with 13 nm side, ensuring minimum 2.5 nm distance between protein complex and walls to minimize any cross talk among protein and its images. Note, water molecules were modeled using TIP3P forcefield. Next, we neutralized the simulation box with Na^+ and Cl^-. Long range electrostatic interactions were captured by Particle Mesh Ewald (PME) method [49]. To model molecular interactions, we started with system energy minimization, then we did NVT and NPT simulations for 100 ps to equilibrate system with V-rescale thermostat (modified Berendsen thermostat) and Berendsen barostat [50]. Finally, we did MD production simulations for 30 ns (time step of 2 fs) with V-rescale thermostat and Parrinello-Rahman barostat [51] and repeated modeling two more times (90 ns in total) to capture statistical behavior. It should be noted that all resulting trajectories were visualized and analyzed with VMD tools.

3.5 Conclusions

PLpro inhibitors have great potential for improving the treatment of SCoV-2. PLpro inhibitors inhibit viral infection via multiple methods and block viral replication and suppress

the production of interferons by infected cells. Up-regulating the production of interferons by SARS-CoV2 infected could have synergistic effects with inhibiting viral replication because it will prevent neighboring cells from being infected with viruses. SCoV-2 has evolved to contain multiple proteins that reduce the production of interferons and enable immune cells evasion, and it is likely that these pathways play essential roles in allowing SCoV-2 to spread efficiently. However, despite their promise developing PLpro inhibitors has been challenging. HTS on PLpro have yielded very few promising leads and existing PLpro inhibitors have shown minimal activity in mice. In contrast, in the case of Mpro inhibitors, multiple classes of inhibitors have been developed that have been successful in a wide variety of animal models and in human clinical trials. There is consequently a great need for the development of new PLpro inhibitors.

In this report, we screened a 115,000-molecule library and identified a new chemical scaffold based on a mercaptopyrimidine fragment that inhibited PLpro activity with IC_{50s} in the low micromolar range, was an RCI, and also inhibited viral replication in cells. Compound 5 is to our knowledge the first example of an RCI that can inhibit PLpro and viral replication in cells. Compound 5 undergoes a nucleophilic aromatic substitution (S_NAr) reaction with thiols in PLpro and reacts in a fundamentally different mechanism than traditional RCIs, which are based upon the reverse Michael addition reaction. RCIs have significant potential as therapeutics because of their ability to inhibit protein activity for long periods of time like covalent inhibitors, but do not induce the toxicity of covalent inhibitors because of their reversible nature. However, developing RCIs is challenging because of the limited number of electrophiles that form reversible bonds with proteins. The mercaptopyridine fragment represents a new scaffold for developing RCIs and should enable the development of RCIs that inhibit the function of new classes of proteins outside of PLPro, which do not perform Michael addition reactions efficiently. In this report we also performed an SAR of compound 5 and identified analogs with lower IC_{50s} and higher stability in the presence of GSH. Collectively, these experiments demonstrate that compound 5 is a promising lead fragment for future development given its efficacy in cells and ability to act as an RCI.

3.6 References

1. Z. Niknam, A. Jafari, A. Golchin, F. Danesh Pouya, M. Nemati, M. Rezaei-Tavirani and Y. Rasmi, *Eur J Med Res*, 2022, **27**, 6.

2. J. Zheng, *Int J Biol Sci*, 2020, **16**, 1678-1685.

3. H. Jiang, P. Yang and J. Zhang, *Frontiers in Chemistry*, 2022, **10**.

4. C. Batista, S. Shoham, O. Ergonul, P. Hotez, M. E. Bottazzi, J. P. Figueroa, S. Gilbert, M. Gursel, M. Hassanain, G. Kang, D. Kaslow, J. H. Kim, B. Lall, H. Larson, D. Naniche, T. Sheahan, A. Wilder-Smith, S. O. Sow, P. Yadav and N. Strub-Wourgaft, *EClinicalMedicine*, 2021, **36**, 100911.

5. L. D. Saravolatz, S. Depcinski and M. Sharma, *Clin Infect Dis*, 2023, **76**, 165-171.

6. K. Rosenke, M. C. Lewis, F. Feldmann, E. Bohrnsen, B. Schwarz, A. Okumura, W. F. Bohler, J. Callison, C. Shaia, C. M. Bosio, J. Lovaglio, G. Saturday, M. A. Jarvis and H. Feldmann, *bioRxiv*, 2022, DOI: 10.1101/2022.09.03.506479.

7. J. H. Jeong, S. Chokkakula, S. C. Min, B. K. Kim, W. S. Choi, S. Oh, Y. S. Yun, D. H. Kang, O. J. Lee, E. G. Kim, J. H. Choi, J. Y. Lee, Y. K. Choi, Y. H. Baek and M. S. Song, *Antiviral Res*, 2022, **208**, 105430.

8. C. K. H. Wong, I. C. H. Au, K. T. K. Lau, E. H. Y. Lau, B. J. Cowling and G. M. Leung, *Lancet*, 2022, **400**, 1213-1222.

9. L. Zhong, Z. Zhao, X. Peng, J. Zou and S. Yang, *Precision Clinical Medicine*, 2022, **5**.

10. S. Lei, X. Chen, J. Wu, X. Duan and K. Men, *Signal Transduction and Targeted Therapy*, 2022, **7**, 387.

11. J. Osipiuk, S. A. Azizi, S. Dvorkin, M. Endres, R. Jedrzejczak, K. A. Jones, S. Kang, R. S. Kathayat, Y. Kim, V. G. Lisnyak, S. L. Maki, V. Nicolaescu, C. A. Taylor, C. Tesar, Y. A. Zhang, Z. Zhou, G. Randall, K. Michalska, S. A. Snyder, B. C. Dickinson and A. Joachimiak, *Nat Commun*, 2021, **12**, 743.

12. D. Shin, R. Mukherjee, D. Grewe, D. Bojkova, K. Baek, A. Bhattacharya, L. Schulz, M. Widera, A. R. Mehdipour, G. Tascher, P. P. Geurink, A. Wilhelm, G. J. van der Heden van Noort, H. Ovaa, S. Müller, K. P. Knobeloch, K. Rajalingam, B. A. Schulman, J. Cinatl, G. Hummer, S. Ciesek and I. Dikic, *Nature*, 2020, **587**, 657-662.

13. A. T. Ton, M. Pandey, J. R. Smith, F. Ban, M. Fernandez and A. Cherkasov, *Trends Pharmacol Sci*, 2022, **43**, 906-919.

14. H. Tan, Y. Hu, P. Jadhav, B. Tan and J. Wang, *J Med Chem*, 2022, **65**, 7561-7580.

15. B. K. Maiti, *ACS Pharmacol Transl Sci*, 2020, **3**, 1017-1019.

16. Y. M. Báez-Santos, S. E. St John and A. D. Mesecar, *Antiviral Res*, 2015, **115**, 21-38.

17. Y. Jiang, K. Tong, R. Yao, Y. Zhou, H. Lin, L. Du, Y. Jin, L. Cao, J. Tan, X. D. Zhang, D. Guo, J. A. Pan and X. Peng, *Cell Biosci*, 2021, **11**, 140.

18. M. Frieman, K. Ratia, R. E. Johnston, A. D. Mesecar and R. S. Baric, *J Virol*, 2009, **83**, 6689-6705.

19. M. A. Clementz, Z. Chen, B. S. Banach, Y. Wang, L. Sun, K. Ratia, Y. M. Baez-Santos, J. Wang, J. Takayama, A. K. Ghosh, K. Li, A. D. Mesecar and S. C. Baker, *J Virol*, 2010, **84**, 4619-4629.

20. D. J. Calleja, G. Lessene and D. Komander, *Front Chem*, 2022, **10**, 876212.

21. L. A. Armstrong, S. M. Lange, V. Dee Cesare, S. P. Matthews, R. S. Nirujogi, I. Cole, A. Hope, F. Cunningham, R. Toth, R. Mukherjee, D. Bojkova, F. Gruber, D. Gray, P. G. Wyatt, J. Cinatl, I. Dikic, P. Davies and Y. Kulathu, *PLoS One*, 2021, **16**, e0253364.

22. X. Gao, B. Qin, P. Chen, K. Zhu, P. Hou, J. A. Wojdyla, M. Wang and S. Cui, *Acta Pharm Sin B*, 2021, **11**, 237-245.

23. Z. Shen, K. Ratia, L. Cooper, D. Kong, H. Lee, Y. Kwon, Y. Li, S. Alqarni, F. Huang, O. Dubrovskyi, L. Rong, G. R. J. Thatcher and R. Xiong, *J Med Chem*, 2022, **65**, 2940-2955.

24. W. Rut, Z. Lv, M. Zmudzinski, S. Patchett, D. Nayak, S. J. Snipas, F. El Oualid, T. T. Huang, M. Bekes, M. Drag and S. K. Olsen, *Sci Adv*, 2020, **6**.

25. Z. Fu, B. Huang, J. Tang, S. Liu, M. Liu, Y. Ye, Z. Liu, Y. Xiong, W. Zhu, D. Cao, J. Li, X. Niu, H. Zhou, Y. J. Zhao, G. Zhang and H. Huang, *Nature Communications*, 2021, **12**, 488.

26. C. Ma, M. D. Sacco, Z. Xia, G. Lambrinidis, J. A. Townsend, Y. Hu, X. Meng, T. Szeto, M. Ba, X. Zhang, M. Gongora, F. Zhang, M. T. Marty, Y. Xiang, A. Kolocouris, Y. Chen and J. Wang, *ACS Cent Sci*, 2021, **7**, 1245-1260.

27. T. Klemm, G. Ebert, D. J. Calleja, C. C. Allison, L. W. Richardson, J. P. Bernardini, B. G. Lu, N. W. Kuchel, C. Grohmann, Y. Shibata, Z. Y. Gan, J. P. Cooney, M. Doerflinger, A. E. Au, T. R. Blackmore, G. J. van der Heden van Noort, P. P. Geurink, H. Ovaa, J. Newman, A. Riboldi-Tunnicliffe, P. E. Czabotar, J. P. Mitchell, R. Feltham, B. C. Lechtenberg, K. N. Lowes, G. Dewson, M. Pellegrini, G. Lessene and D. Komander, *Embo j*, 2020, **39**, e106275.

28. K. Ratia, S. Pegan, J. Takayama, K. Sleeman, M. Coughlin, S. Baliji, R. Chaudhuri, W. Fu, B. S. Prabhakar, M. E. Johnson, S. C. Baker, A. K. Ghosh and A. D. Mesecar, *Proc Natl Acad Sci U S A*, 2008, **105**, 16119-16124.

29. B. T. Freitas, I. A. Durie, J. Murray, J. E. Longo, H. C. Miller, D. Crich, R. J. Hogan, R. A. Tripp and S. D. Pegan, *ACS Infect Dis*, 2020, **6**, 2099-2109.

30. H. Shan, J. Liu, J. Shen, J. Dai, G. Xu, K. Lu, C. Han, Y. Wang, X. Xu, Y. Tong, H. Xiang, Z. Ai, G. Zhuang, J. Hu, Z. Zhang, Y. Li, L. Pan and L. Tan, *Cell Chem Biol*, 2021, **28**, 855-865.e859.

31. Y. Zhao, X. Du, Y. Duan, X. Pan, Y. Sun, T. You, L. Han, Z. Jin, W. Shang, J. Yu, H. Guo, Q. Liu, Y. Wu, C. Peng, J. Wang, C. Zhu, X. Yang, K. Yang, Y. Lei, L. W.

Guddat, W. Xu, G. Xiao, L. Sun, L. Zhang, Z. Rao and H. Yang, *Protein Cell*, 2021, **12**, 877-888.

32. Z. Jin, X. Du, Y. Xu, Y. Deng, M. Liu, Y. Zhao, B. Zhang, X. Li, L. Zhang, C. Peng, Y. Duan, J. Yu, L. Wang, K. Yang, F. Liu, R. Jiang, X. Yang, T. You, X. Liu, X. Yang, F. Bai, H. Liu, X. Liu, L. W. Guddat, W. Xu, G. Xiao, C. Qin, Z. Shi, H. Jiang, Z. Rao and H. Yang, *Nature*, 2020, **582**, 289-293.

33. S. Yuan, X. Gao, K. Tang, J. P. Cai, M. Hu, P. Luo, L. Wen, Z. W. Ye, C. Luo, J. O. Tsang, C. C. Chan, Y. Huang, J. Cao, R. Liang, Z. Qin, B. Qin, F. Yin, H. Chu, D. Y. Jin, R. Sun, J. F. Chan, S. Cui and K. Y. Yuen, *Protein Cell*, 2022, **13**, 940-953.

34. P. Kittakoop, D. Darshana, R. Sangsuwan and C. Mahidol, *Heterocycles: an international journal for reviews and communications in heterocyclic chemistry*, 2022, **105**, 115-146.

35. D. Murugesan, P. C. Ray, T. Bayliss, G. A. Prosser, J. R. Harrison, K. Green, C. Soares de Melo, T. S. Feng, L. J. Street, K. Chibale, D. F. Warner, V. Mizrahi, O. Epemolu, P. Scullion, L. Ellis, J. Riley, Y. Shishikura, L. Ferguson, M. Osuna-Cabello, K. D. Read, S. R. Green, D. A. Lamprecht, P. M. Finin, A. J. C. Steyn, T. R. Ioerger, J. Sacchettini, K. Y. Rhee, K. Arora, C. E. Barry, 3rd, P. G. Wyatt and H. I. M. Boshoff, *ACS Infect Dis*, 2018, **4**, 954-969.

36. S. Wang, Y. Tian, M. Wang, M. Wang, G. B. Sun and X. B. Sun, *Front Pharmacol*, 2018, **9**, 353.

37. T. A. Baillie, *Angew Chem Int Ed Engl*, 2016, **55**, 13408-13421.

38. J. M. Bradshaw, J. M. McFarland, V. O. Paavilainen, A. Bisconte, D. Tam, V. T. Phan, S. Romanov, D. Finkle, J. Shu, V. Patel, T. Ton, X. Li, D. G. Loughhead, P. A. Nunn, D. E. Karr, M. E. Gerritsen, J. O. Funk, T. D. Owens, E. Verner, K. A. Brameld, R. J. Hill, D. M. Goldstein and J. Taunton, *Nat Chem Biol*, 2015, **11**, 525-531.

39. E. Resnick, A. Bradley, J. Gan, A. Douangamath, T. Krojer, R. Sethi, P. P. Geurink, A. Aimon, G. Amitai, D. Bellini, J. Bennett, M. Fairhead, O. Fedorov, R. Gabizon, J. Gan, J. Guo, A. Plotnikov, N. Reznik, G. F. Ruda, L. Díaz-Sáez, V. M. Straub, T. Szommer, S. Velupillai, D. Zaidman, Y. Zhang, A. R. Coker, C. G. Dowson, H. M. Barr, C. Wang, K. V. M. Huber, P. E. Brennan, H. Ovaa, F. von Delft and N. London, *J Am Chem Soc*, 2019, **141**, 8951-8968.

40. R. Kooij, S. Liu, A. Sapmaz, B. T. Xin, G. M. C. Janssen, P. A. van Veelen, H. Ovaa, P. T. Dijke and P. P. Geurink, *J Am Chem Soc*, 2020, **142**, 16825-16841.

41. A. Birkholz, D. J. Kopecky, L. P. Volak, M. D. Bartberger, Y. Chen, C. M. Tegley, T. Arvedson, J. D. McCarter, C. Fotsch and V. J. Cee, *J Med Chem*, 2020, **63**, 11602-11614.

42. B. Hess, C. Kutzner, D. van der Spoel and E. Lindahl, *J Chem Theory Comput*, 2008, **4**, 435-447.

43. K. Vanommeslaeghe, E. Hatcher, C. Acharya, S. Kundu, S. Zhong, J. Shim, E. Darian, O. Guvench, P. Lopes, I. Vorobyov and A. D. Mackerell, Jr., *J Comput Chem*, 2010, **31**, 671-690.

44. N. M. O'Boyle, M. Banck, C. A. James, C. Morley, T. Vandermeersch and G. R. Hutchison, *J Cheminform*, 2011, **3**, 33.

45. K. Vanommeslaeghe and A. D. MacKerell, Jr., *J Chem Inf Model*, 2012, **52**, 3144-3154.

46. O. Guvench, E. R. Hatcher, R. M. Venable, R. W. Pastor and A. D. Mackerell, *J Chem Theory Comput*, 2009, **5**, 2353-2370.

47. W. Yu, X. He, K. Vanommeslaeghe and A. D. MacKerell, Jr., *J Comput Chem*, 2012, **33**, 2451-2468.

48. W. Humphrey, A. Dalke and K. Schulten, *J Mol Graph*, 1996, **14**, 33-38, 27-38.

49. B. Kohnke, C. Kutzner and H. Grubmüller, *J Chem Theory Comput*, 2020, **16**, 6938-6949.

50. M. Bernetti and G. Bussi, *J Chem Phys*, 2020, **153**, 114107.

51. Q. Ke, X. Gong, S. Liao, C. Duan and L. Li, *Journal of Molecular Liquids*, 2022, **365**, 120116.

3.7 Acknowledgments

Conceptualization, N. M., J. S., M. O., D. N. and M. R. K. M.; methodology, T. B., E. W., R. K. S, E. K., K. S. P., K. B., Z. K., U. S.-G., G. R. K.; software, T. B. and N. M.; validation, T. B., N. M.; formal analysis, T. B., E. W., R. K. S, E. K., K. S. P., K. B., Z. K., G. R. K.; investigation, T. B. and N. M.; resources, N. M., J. S., M. O., D. N., M. R. K. M.; data curation, N. M. and T. B.; writing – original draft preparation, T. B. and N. M.; writing – review and editing, N. M., T. B., J. S., G. R. K., R. S.; visualization, T. B.; supervision, N. M., J. S., M. O.; project administration, N. M.; funding acquisition, N. M., M. O., J. S. All authors have read and agreed to the published version of the manuscript.

This chapter has been published, entitled as Mercapto-pyrimidines are reversible covalent inhibitors of the papain-like protease and inhibit SARS-CoV-2 (SCoV-2) replication in RSC Advances (Bajaj and Wehri et. al., 2023)

I acknowledge all advisors and researchers, Niren Murthy and Kundan S. Pardeshi, Julia Schaletzky and Eddie Wehri, Melanie Ott, Renuka Kumar, Ursula Schulze-Gahmen and Rahul Suryawanshi, Daniel K. Nomura and Elizabeth King, Mohammad R.K. Mofrad, Kamyar Behrouzi and Zahra Khodabakshi for supporting this project in numerous ways including, conceiving this project, screening of chemical libraries, testing hits in BSL3 conditions, characterizing and computational efforts, respectively.

Chapter 4

Discovery of covalent inhibitors against Non-structural protein 15 (Nsp15) from SARS-CoV-2 (SCoV-2)

4.1 Abstract

Non-structural protein 15 (Nsp15) is a uridylate-specific endoribonuclease and is a promising therapeutic target for drug development to combat the SARS-CoV-2 (SCoV-2) virus. However, developing inhibitors against Nsp15 has been challenging due to the larger binding surface. We performed a series of high throughput screening assays with 2640 acrylamide-based compounds against Nsp15 to identify those fragments that could bind to cysteine residue and inhibit the endoribonuclease activity of Nsp15. Ten compounds were selected that inhibited Nsp15 irreversibly with IC_{50} less than 5 µM. These compounds show drug-like properties including low molecular weight (180-300 g/mol), logP (less than 3), zero violations to Lipinski's rule and no PAINS alert. Collectively, these results demonstrate that acrylamide fragments are promising class of compounds for developing Nsp15 inhibitors and their optimal physiochemical and drug-likeness properties highlight its great potential for optimizing and developing into promising antiviral drug candidates.

4.2 Introduction

The emergence and rapid spread of the SCoV-2 virus have stimulated the need for new drugs. Hundreds of drug discovery campaigns have been run to target essential proteins from SCoV-2 virus[1, 2]. Targeting RdRp[3] and Mpro[4, 5] has led to the discovery of several promising antiviral drugs, however, alternative drugs that target other crucial proteins from SCoV-2 are still needed[6, 7]. The non-structural protein 15 (Nsp15) is a promising therapeutic target candidate for drug development to combat SCoV-2 because its inhibition results in the upregulation of interferons, which protects against viral infections[8, 9].

Nsp15 cleaves viral RNA and suppresses host sensors that recognize viral RNA and induce the production of interferons[10]. Inhibition of Nsp15 activates the production of interferon and prevents the spread of viral infection through paracrine signaling[11]. For example, infection of lung-derived epithelial cell lines and primary nasal epithelial air-liquid interface (ALI) cultures with mutant Nsp15 SCoV-2 caused increased secretion of interferons and attenuated viral replication significantly[12]. In another instance, infection of mutant Nsp15 MHV coronavirus to mouse bone marrow-derived macrophages resulted in an early and robust induction of interferon leading to rapid cell death. This suggests that viruses with mutant Nsp15 cannot infect mice effectively, due to their activation of the host immune response[8], suggesting that Nsp15 inhibition will have a therapeutic effect against SCoV-2. Additionally, Nsp15 is also an evolutionary conserved protein[13], therefore, drugs against SCoV-2 Nsp15 could also be potential drugs for other coronaviruses and nidoviruses. Though Nsp15 has great potential as a drug target, it is less explored in terms of drug discovery due to the challenge of drugging the large binding interface[14]. Only a handful of compounds have been identified that can inhibit Nsp15.

To drug the undruggable proteins, targeted covalent inhibition could be a promising route. SCoV-2 Nsp15 has several free cysteines that play a role in subunit oligomerization and interactions with the RNA substrate[15] and can be potentially targeted by covalent drugs. Alkylation of these cysteines with covalent drugs has the potential to inhibit Nsp15.

In this report, we screened an acrylamide-based electrophile library of 2640 compounds against Nsp15 and identified several acrylamides as covalent inhibitors of Nsp15 with IC_{50} less than 5 µM. Acrylamides have shown higher selectivity with cysteine and moderate reactivity to thiols at the physiological pH. Their specificity towards Nsp15 demonstrated them as interesting lead compounds for future drug discovery campaigns against coronaviruses. These compounds only not serve as initial hits, but also, they are drug-like candidates that follow Lipinski's rule of five, high oral bioavailability, easy to synthesize, therefore bringing a new platform for drug discovery of RNA binding proteins. Biophysical experiments showed that one of these ten compounds modified the cysteine next to the active site.

4.3 Results and discussion

Selecting acrylamide library to discover covalent inhibitors against SCoV-2 Nsp15

To discover the covalent inhibitors that could sustain engagement efficiently with minimum off-target reactivity, we targeted the most nucleophilic residues that are cysteine residues[16] in Nsp15. The most used electrophile building block as a covalent inhibitor targeting cysteines are Michael acceptor, such as acrylamides[17]. Acrylamides have been widely used as electrophiles for irreversibly covalent inhibitors for many proteins bearing non-catalytic cysteine, for example, afatinib[18], ibrutinib[19], and AMG-510[20] are acrylamide-based inhibitors

of EGFR, BTK, and K-RasG12C, respectively[21]. We used an electrophile library containing 2640 acrylamide compounds from Enamine.

Acrylamide-based compounds as covalent inhibitors against SCoV-2 Nsp15

The hexameric Nsp15 was recombinantly expressed and purified from bacterial cells using talon and size exclusion chromatography[13]. We utilized two parameters (binding and inhibiting Nsp15) to discover acrylamide-based covalent inhibitors from high throughput screening (Fig. 4.1A). We used an activity-based protein profiling (ABPP) probe, cysteine-reactive tetramethylrhodamine-5-iodoacetamide dihydroiodide (IA-Rho)[22] in a competitive manner to screen acrylamide library to facilitate the discovery of covalent ligands against SCoV-2 Nsp15. The presence of cysteine-reactive compounds was expected to correspond with disappearance of IA-Rho labeled Nsp15 band. We optimized the Nsp15 and IA-Rho concentrations to 0.25 µg and 0.5 µM, respectively. In the absence of compound, DMSO was added that served as a negative control. We screened 2640 acrylamide-based compounds at the concentration of 40 µM and the compounds that led to disappearance of Nsp15 band, followed by confirmation. The preliminary screening of the acrylamide library resulted in 829 initial hits that showed binding with Nsp15 through cysteine, presenting the hit rate of 31.4%.

To further find out Nsp15 inhibitors, we used a fluorescent-based HTS assay that used a DNA-RNA hybrid oligomer with FRET pair on ends. Endonuclease cleavage of oligomer by Nsp15 was quantified by measuring the fluorescence after exciting at 485 nm and measuring the emission at 535 nm[23]. FRET assay resulted in 408 compounds (hit rate of 15.4%) that inhibited the endonuclease activity of Nsp15 up to 70%. To rule out the false positives, an orthogonal assay was performed to find out if these compounds could prevent mRNA degradation by Nsp15. mRNA degradation assay confirmed the hits inhibiting the 100% activity of Nsp15 and reduced the count to 308 (hit rate of 11.6%).

To narrow down the hit number for potent covalent inhibitors, all three assays were repeated at the concentration of 10 µM further reducing the count to 60 compounds (hit rate of 2%). Sixty compounds were repurchased and validated using all three assays at the concentration of 40 and 10 µM resulting in the discovery of 15 covalent inhibitors against Nsp15. A dose-response fluorescent-based assay that used RNA substrate[13] was performed to validate and select potent inhibitors that selected 10 compounds with IC_{50} less than 5 µM (Fig. 4.1B and Fig. 4.2).

Acrylamide-based Nsp15 covalent inhibitors are non-toxic

To be effective as a drug, a potent molecule must be reactive towards its target in the body in sufficient concentration and stay there in a bioactive form long enough for the expected biological events to occur. Therefore, we assessed the thiol reactivity of these electrophiles

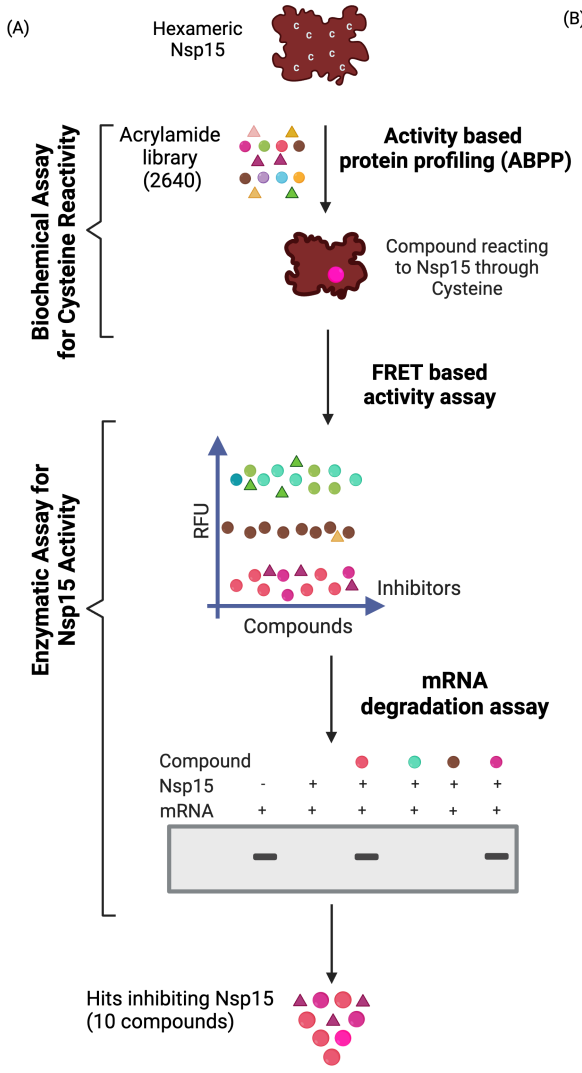

(B)

Compound	IC_{50} (μM)	Chemical Structure
1	1.50	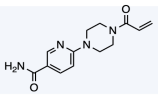
2	4.72	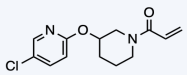
3	1.64	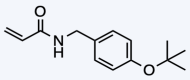
4	3.46	
5	1.11	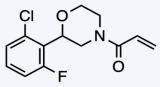
6	1.48	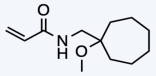
7	3.22	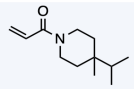
8	2.21	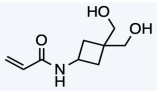
9	0.99	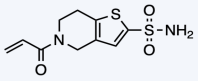
10	3.16	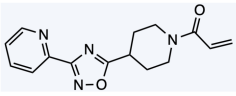

Figure 4.1: HTS of acrylamide library consisting of 2640 compounds against Nsp15 identified ten inhibitors with sub-micromolar IC_{50}s.

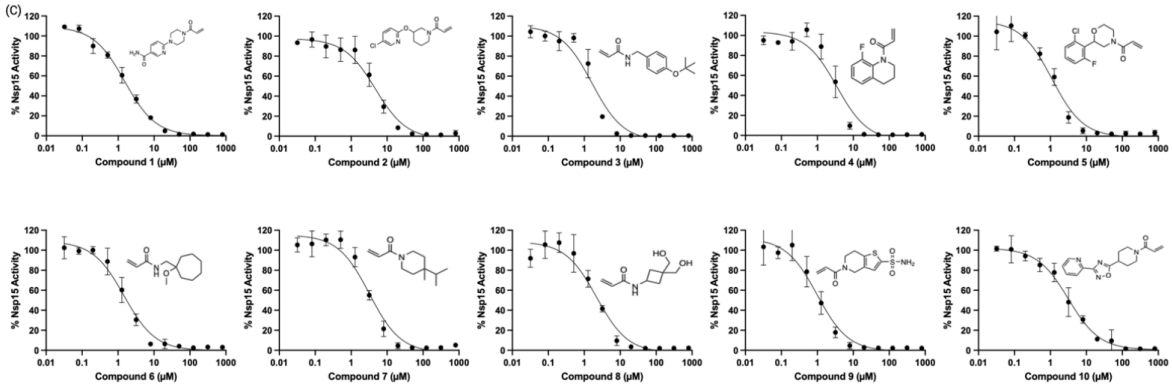

Figure 4.2: Dose response curves and chemical structures of ten compounds that were fished out from high throughput screening of acrylamide library of 2640 compound as covalent inhibitors of SCoV-2 Nsp15.

by incubating with reduced Ellman's reagent (5,5 -dithio-bis-2-nitrobenzoic acid (DTNB)), following the absorbance of TNB^{2-} at the 412 nm wavelength for up to 5 hours[24] (Fig. 4.3A). To measure the kinetic constants and evaluate the intrinsic reactivity of these acrylamide-based Nsp15 towards thiols, we fitted the data to a second-order reaction rate equation and extrapolated the kinetic constant for the alkylation by acrylamide-based inhibitors. All compounds showed an excellent fit to the kinetic model of one-phase exponential decay (R^2 ¿ 0.9). The kinetic rate constant (k) for Nsp15 inhibitors ranged from 1.5-4 $M^{-1}s^{-1}$ (Fig. 4.4). These rate constant values suggest that these compounds have high intrinsic reactivity towards thiols (or cysteines in Nsp15). Though promiscuity does not correlate with reactivity, the high reactivity of the compounds could define the instability of the compounds and lead to cytotoxicity in cells[24]. Therefore, next, we assessed drug toxicity which is one of the key parameters in clinical pharmacology during preclinical screening of drug candidates[25]. To assess the drug response and toxicity, a resazurin assay was used to analyze the cell viability[26] due to these Nsp15 inhibitors. A range of concentrations (0.03-0.5 mM) of inhibitors were tested on Caco-2 cells (*in vitro* model of the intestinal epithelial cells), cell viability was measured and CC_{50} was calculated (Fig. 4.3C). At the lower concentration (0.3-0.125 mM), most of the compounds (except compound 5) show 100% cell viability suggesting no toxicity. At the higher concentration (0.25-1 mM), compounds 1, 2, 3, 8, and 10 show cell viability greater than 85% and rest less than 40%.

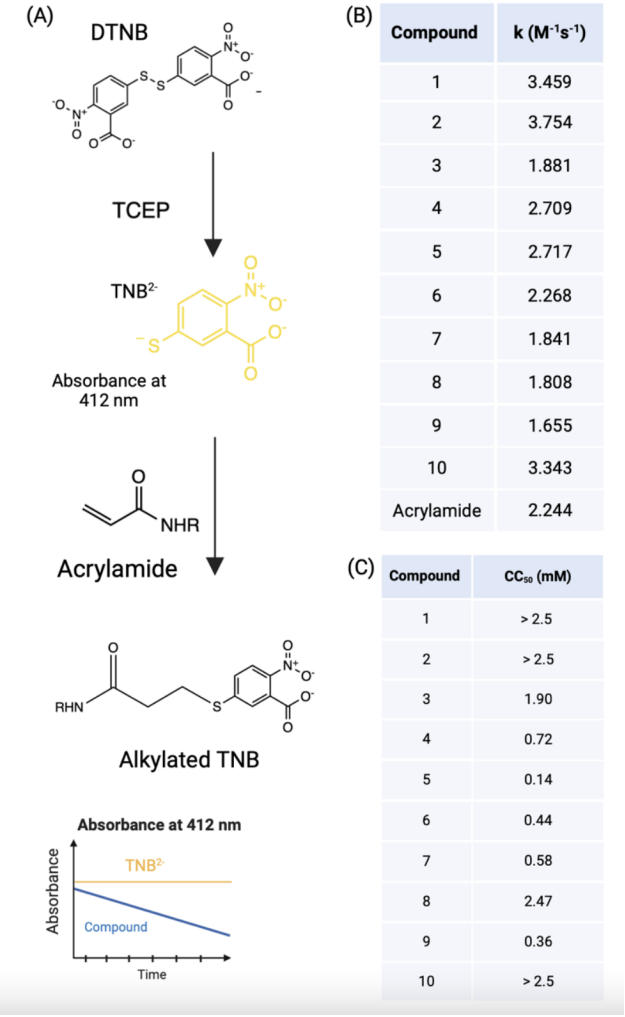

(B)

Compound	k ($M^{-1}s^{-1}$)
1	3.459
2	3.754
3	1.881
4	2.709
5	2.717
6	2.268
7	1.841
8	1.808
9	1.655
10	3.343
Acrylamide	2.244

(C)

Compound	CC_{50} (mM)
1	> 2.5
2	> 2.5
3	1.90
4	0.72
5	0.14
6	0.44
7	0.58
8	2.47
9	0.36
10	> 2.5

Figure 4.3: Characterization of thiol reactivity of acrylamide-based Nsp15 covalent inhibitors.

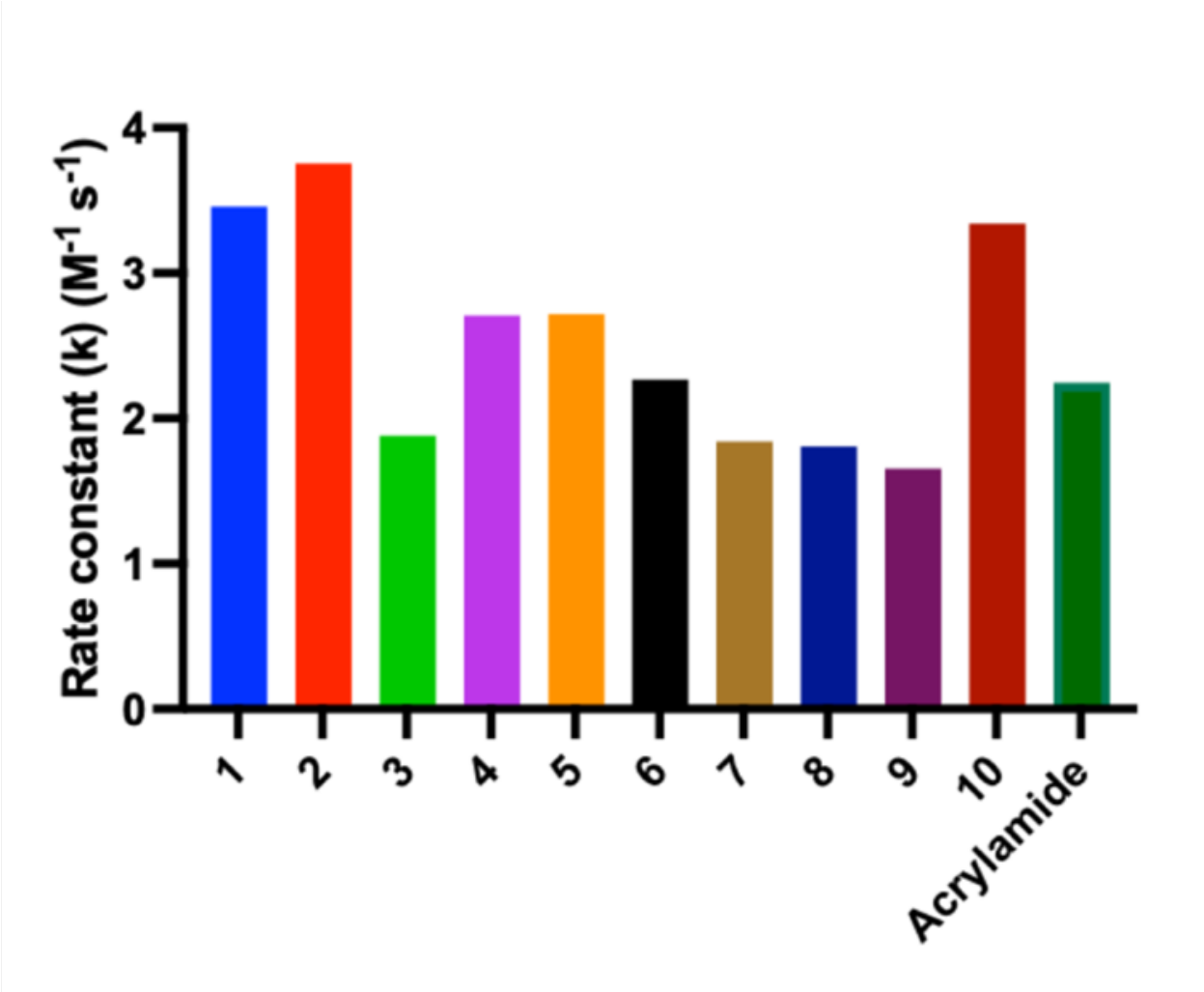

Figure 4.4: Calculated the rate constant (k) of reactivity of ten compounds towards thiols and compared it with acrylamide.

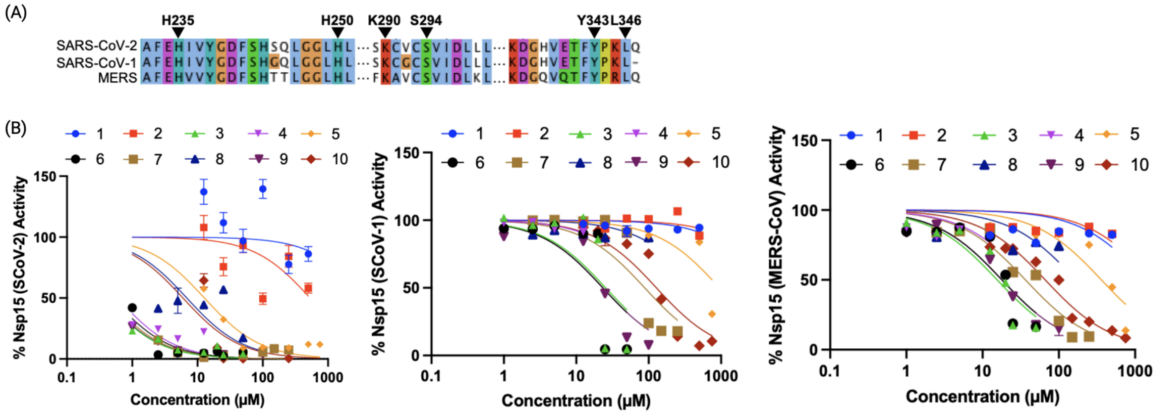

Figure 4.5: Efficacy of covalent Nsp15 inhibitors against other coronaviruses (SCoV-2, SCoV-1 and MERS-CoV).

Selectivity of inhibitors against Nsp15 homologs and unrelated proteins

Nsp15 is an evolutionary conserved protein and is called a genetic marker for nidoviruses. Conservation of Nsp15 across species suggests that SCoV-2 Nsp15 inhibitors might be also used to target Nsp15 from other coronaviruses. SCoV-2 Nsp15 shares the sequence identity with other coronavirus species, SCoV-1, and Middle East respiratory syndrome coronavirus (MERS-CoV) with the percentage of 88.44% and 51.47%, respectively (Fig. 4.5A)[15]. We wondered if these ten compounds could also inhibit Nsp15 from SCoV-1 and MERS-CoV. We tested the inhibitory activity of these compounds against Nsp15 from SCoV-2, SCoV-1, and MERS-CoV using a fluorescent-based endonuclease assay[15]. We observed that compounds inhibited SCoV-1 and MERS-CoV Nsp15, however, with different extents. A dose-response assay was performed to determine the IC_{50} values of these compounds against Nsp15 from SCoV-2, SCoV-1, and MERS-CoV (Fig. 4.6A and Fig. 4.5B). This suggests that these acrylamide compounds could be initial hits to improve and design potent compounds against coronaviruses.

One step forward to test the specificity, we also tested these ten compounds against a distantly related RNA endonuclease, RNase A that shares a similar catalytic mechanism with Nsp15. We observed that none of these inhibitors inhibited RNase A activity, suggesting inhibitors are not acting through the catalytic triad, as expected (RNase A and Nsp15 share the catalytic triad). At last, we also tested these compounds against SIRT1, an unrelated enzyme that contains nucleophilic cysteine to get nitrosylated. As expected, and hypothesized, none of the compounds inhibited SIRT1 enzymatic activity suggesting nucleophilic cysteine in SIRT1 were not being alkylated by acrylamide-based Nsp15 inhibitors. In conclusion, these acrylamide-based compounds are specific inhibitors of Nsp15 from coronaviruses (Fig.

(A)

Compound	SCoV-2 (IC_{50}(μM))	SCoV-1 (IC_{50}(μM))	MERS-CoV (IC_{50}(μM))
1	3977	5129	1375
2	533	7876	1682
3	0.368	25.46	15.53
4	0.596	117.2	40.74
5	12.77	952.6	361.6
6	0.496	23.32	17.96
7	0.420	88.18	36.48
8	6.8	508.3	167.6
9	0.383	23.36	17.86
10	8.415	189.4	107.0

(B)

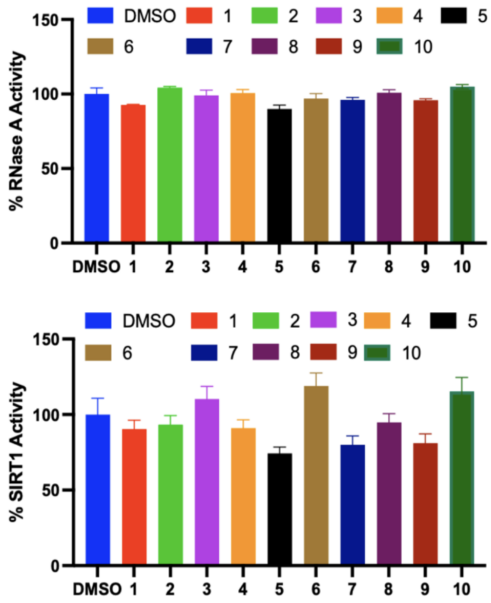

Figure 4.6: Efficacy of covalent Nsp15 inhibitors against related and unrelated enzymes.

4.6B).

The ability of acrylamide-based inhibitors to inhibit Nsp15 in cells

To test the inhibitory effect of these *in vitro* Nsp15 inhibitors in a cellular environment, we utilized an immunological assay based on a genetic ablation of Nsp15 activity resulting in higher production of IFN- at 48 hours post-infection (hpi)[8]. With catalytic-inactive mutant (H234A) Nsp15 as a positive control, we evaluated ten compounds in the Caco2-AT culture system. All the compound-treated cells did not produce more IFN- compared to the untreated wild-type (WT) group, and some even produced less than the WT group. The viral nucleocapsid (N) gene levels of all tested samples are comparable, indicating that all the cells were successfully infected (Fig. 4.7). These results suggest that these ten compounds have no significant inhibitory effect on Nsp15 activity in the Caco2-AT test system. In future studies, we need to synthesize more effective compounds that can inhibit Nsp15 activity or develop more sensitive detection methods to detect decreased Nsp15 activity.

Nsp15 covalent inhibitors have drug-likeness

Estimation of the pharmacokinetic profile of a drug candidate is a crucial aspect of drug

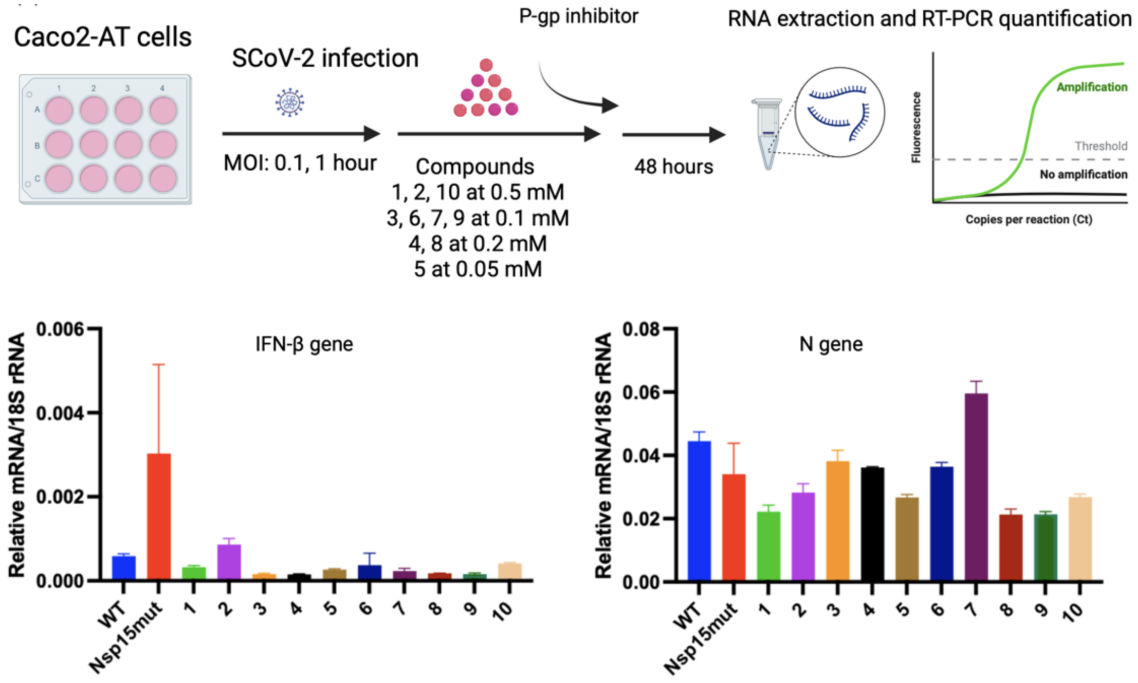

Figure 4.7: Assessment of Nsp15 inhibitors in SCoV-2 infected Caco2-AT cells.

development that includes parameters like its absorption, distribution, metabolism, and excretion (ADME)[27]. In this report, we theoretically predicted the ADME parameters of these inhibitors using SwissADME[28, 29], a free and readily accessible web tool to gain the insights regarding effectivity of these Nsp15 inhibitors as an oral drug. We predicted the physiochemical properties, pharmacokinetics, drug-likeness, and medicinal chemistry friendliness of these small molecules by importing the 2D structures into the webpage interface in canonical simplified molecular input line entry system (SMILES) format.

The ability of a drug to move across the membranes for transportation throughout the body is highly dependent on its physiochemical properties[30, 31]. All Nsp15 inhibitors exhibited the optimal values of all physiochemical properties, indicating good oral bioavailability, suggesting them as a potential drug candidate[32] (Fig. 4.7B). SwissADME can also predict gastrointestinal (GI) absorption and blood-brain barrier (BBB) penetration[33], two pharmacokinetic behaviors associated with lipophilicity and polarity of the molecules. While all acrylamide-based Nsp15 inhibitors were predicted to have a high level of GI absorption, six out of ten inhibitors showed a probability of crossing the BBB. Interestingly, all these inhibitors are indicated as non-inhibitors of P-glycoprotein (P-gp), suggesting that they are unlikely to be effluxed from cells.

Drug-likeness is an essential aspect of drug development that evaluates the potential of

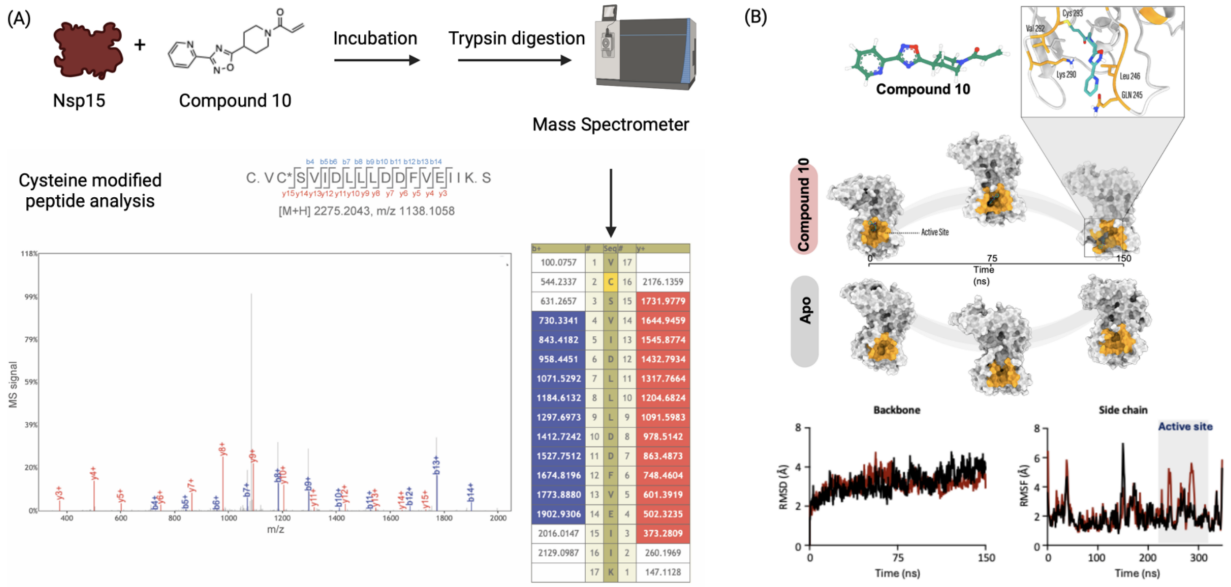

Figure 4.8: Compound 10 modifies Cys293 residue from Nsp15.

a molecule to become an oral drug[34]. These ten inhibitors followed Lipinski's rule of five[35], with zero violations and a bioavailability score of 0.55, suggesting a chance for a molecule to become an oral drug with respect to bioavailability (drug-likeness)[36]. Nsp15 inhibitors have shown 0 alerts of being promiscuous compounds through the PAINS score. Additionally, these compounds are very easy to synthesize (Fig. 4.7A).

Compound 10 modified cysteine in C-domain of Nep15

To determine the cysteine residue as a site of covalent interaction of Nsp15 and compounds, we performed tandem mass spectrometry (MS/MS) analysis of the protein-compound complex subjected to trypsin digestion. Tandem mass spectrometry revealed that compound 10 is covalently reacting to Cys293. Cys293 is present in the C-terminal domain of Nsp15, next to the catalytic core of Nsp15 determining the endoribonuclease activity[15]. Cys293 has been also observed in interaction with Favipiravir drug through van der walls interactions in molecular docking[37] (Fig. 4.8A). To assess the structural dynamics of Nsp15 following the irreversible covalent binding of compound 10 to Cys293 via a thiol-Michael addition, we conducted molecular dynamics (MD) simulations of Nsp15 in its apo form and in complex with compound 10 (covalently bound to Cys293). Structural analysis from the MD simulations revealed that the irreversible binding of compound 10 to Nsp15 significantly distorts the active site (Fig. 4.8B). Although there is no observable change in the overall backbone of Nsp15, the side chain fluctuations in the compound 10-bound complex are altered, indicating

a distortion of the binding site.

4.4 Experimental

Materials and Methods

Expression and purification of Nsp15

The plasmid expressing SCoV-2 Nsp15 (6X-His-Thrombin-TEV-Nsp15 in pET-14b vector) was a kind gift from Robin Stanley, NIH. SCoV-2 Nsp15 was expressed as described in Pillon et al. Briefly, the plasmid was transformed into C41 (DE3) competent cells and selected on carbenicillin LB agar plates. The next day, a colony was picked to grow a primary culture of 10 mL 2XYT media supplemented with 50 µg/mL carbenicillin. The secondary culture was grown by diluting primary culture 1:100 in 2XYT media to an OD of 1.0 (A_{600}). SCoV-2 Nsp15 protein was expressed with 0.2 M isopropyl -D-1- thiogalactopyranoside (IPTG) for 3 hours at 37 °C. The culture was harvested and resuspended in lysis buffer (50 mM Tris pH 8.0, 500 mM NaCl, 5% glycerol) supplemented with EDTA-free protease inhibitor tablets. The cells were sonicated, and lysate was clarified at 13,000 x g for 30 minutes at 4 °C. The supernatant was loaded on Talon HP column (Cytiva) at the speed of 1 mL/min. The non-specific protein was removed by washing the column with lysis buffer supplemented with 10 mM imidazole. Nsp15 was eluted with high imidazole buffer (lysis buffer supplemented with 250 mM Imidazole). The eluted fractions of Nsp15 were pooled, concentrated, and dialyzed against SEC buffer (20 mM HEPES pH 7.3, 150 mM NaCl, 5 mM $MnCl_2$, 5 mM beta-mercaptoethanol (-me)). The protein was stored in -80 °C until further use.

SCoV-1 and MERS-CoV Nsp15 variants were purified as previously described. Briefly, BL21(DE3) pLYsS cells were transformed with pet28B+ plasmids encoding for these Nsp15 variants. Starter cultures were grown overnight at 37 °C in terrific broth (TB) in the presence of 100 µg/mL kanamycin. Larger cultures of TB-Kanamycin were inoculated with starter culture and grown to an OD 600 nm of 0.6. Cultures were then cooled at 4 °C for 30 minutes before induction with 1 mM IPTG at 16 °C for 20 hours. Cells were then pelleted at 6,000g for 20 mins at 4 °C and resuspended in lysis buffer (20 mM Tris pH 8.0, 150 mM NaCl, 5 mM Imidazole, 0.1% Triton X-100, 1 mg/mL Lysozyme) supplemented with EDTA-free Roche Complete Ultra protease inhibitor tablet (Sigma), 1 mM PMSF and 1 mM beta-mercaptoethanol. The lysate was incubated on ice for 30 minutes before sonication with a Bronson digital Sonifier at 25% amplitude (15 seconds on, 1 minute off) for 10 pulses. Debris was pelleted via centrifugation at 20,000g and the clarified lysate was incubated with Ni-NTA beads (Qiagen) at 4 °C for 4 hours with gentle rotation. The beads were washed in 20 mM Tris pH 8.0, 300 mM NaCl, 10 mM imidazole, 0.01% Triton X-100, and 1 mM beta-mercaptoethanol. The proteins were eluted by incubating the beads with 10-250 mM Imidazole. Fractions were analyzed for purity via SDS-PAGE and staining with Coomassie Brilliant Blue R-250 (BioRad). Pooled fractions were concentrated with a Pierce Protein concentrator 10K (Thermofisher). The buffer was exchanged during concentration with 20 mM 30 HEPES, pH 7.5, 150 mM NaCl, 0.1 mM DTT, and 10% glycerol. Concentrated

protein was aliquoted and stored at 80 °C until usage. Protein concentration was measured using the DTT-resistant Pierce 660 nM Protein BCA Assay kit (Thermofisher).

Activity-based protein profiling to find cysteine binders

The cysteine-reactive compounds against Nsp15 were fished out using ABPP that used IA-Rho to alkylate cysteine present in Nsp15. In the total reaction volume of 25 µL, 0.25 µg of Nsp15 was incubated with 40 µM or 10 µM of the compound for 30 minutes at 37°C. In the absence of a compound, DMSO was added as a negative control. After incubation, 0.5 µM of IA-Rho was added and incubated for 30 minutes in the dark at room temperature. The reaction was stopped using 10 µL of SDS loading buffer and 12.5 µL of the sample was loaded on tris-glycine gel. The gel was imaged under rhodamine fluorescence. The compounds that led to the disappearance of rhodamine-labelled Nsp15 protein bands were taken as Nsp15 cysteine binders.

Fluorescent assay to determine the activity of the Nsp15

The fluorescent-based Nsp15 activity assay was optimized in 384 well plate. The DNA-RNA hydrid substrate (5' FAM- dArUdAdA-TAMRA-3') was custom-ordered from Creative Biogene. The final reaction volume of 25 µL consisted of 12.5 µL of Nsp15 protein (5 nM) and Nsp15 substrate (1 µM) diluted in cleavage buffer (20 mM HEPES pH 7.5, 100 mM NaCl, 5 mM $MnCl_2$) with 2% DMSO (absence and presence of compound (40 and 10 µM)). The Nsp15 activity was monitored by measuring fluorescent intensity at given wavelengths (excitation: 485 nm and emission: 535 nm). The data was analyzed in CDD vault analysis servers. The dose-response assay was performed to determine the IC_{50}s. The experiments were run in duplicates.

mRNA degradation assay

In mRNA degradation assay, 500 ng of Nsp15 was incubated with compound (40 and 10 µM) (2% DMSO in the absence of compound) for 30 minutes in the 25 µL of the buffer (20 mM HEPES pH 7.5, 100 mM NaCl, 5 mM -me, 5 mM $MnCl_2$) at room temperature. After incubation, the Fluc mRNA (0.3 µg) (Trilink) was added to the pre-incubated Nsp15 and allowed the degradation of mRNA for 30 minutes. The RNA loading dye was added and ran on 1% agarose gel. The negative control (mRNA in the absence of Nsp15 and compounds) was also included. The compounds that prevented the mRNA degradation were taken as Nsp15 inhibitors.

Specificity assay

Nsp15 and RNaseA Activity assay

An adapted FRET-based assay was used as previously described[15] employing an RNA substrate with the sequence: 5'FAM-CAACUAAACGAAC-BHQ1'3 where FAM and BHQ1 are 6-Carboxyfluorescein and Black Hole Quencher respectively. The reactions were done in black 96-well polystyrene plates (Greiner, Bio-One) in a 60 µL volume. The reactions contained 60 ng of protein, 1x reaction buffer (25 mM HEPES pH 7.50, 50 mM NaCl, 5 mM $MnCl_2$), and various concentrations of compounds all dissolved in DMSO and were preincubated together in the dark for 30 minutes at RT. RNA substrate was then added to a final concentration of 1 µM and plates were incubated at 37°C for a further 20 minutes. Fluorescence data was collected using a Varioskan LUX plate reader using Excitation and Emission wavelengths of 495 and 520 nm respectively. The results shown are the average of 3 biological replicates +/- SD.

SIRT1 Fluor De Lys Activity assay

SIRT1 activity was measured using the FLUOR DE LYS® SIRT1 fluorometric drug discovery assay kit (Enzo Life Sciences). Recombinant SIRT1 was purified as described in the protein purification methods above. SIRT1, FdL substrate, and NAD+ were used at final concentrations of 200 nM, 25 µM, and 5 mM, respectively. Inhibitor compounds were preincubated with SIRT1 in the absence of NAD+ or FdL Substrate for 30 minutes at 25 °C. The reactions were then allowed to proceed for 30 minutes at 37 °C following the addition of substrate. The reactions were terminated by the addition of developer reagent and incubated for 15 minutes at room temperature in the dark before being measured on a spectrophotometer using Excitation and Emission wavelengths of 360 and 460 nm respectively on a Varioskan LUX plate reader. The results shown are the average of 3 biological replicates +/- SD.

Cell lines and virus

A Caco-2 cell line expressing hACE2 and hTMPRSS2 (Caco2-AT) (1), a gift from Dr. Mohsan Saeed (Boston University), was propagated in DMEM containing 10% FBS, 1% Pen/Strep, 1×NEAA, 1 g/mL puromycin (InVivogen, ant-pr-05), and 1 g/mL blasticidin (InVivogen, ant-bl-05). A Vero E6 line expressing hACE2 and hTMPRSS2 (Vero-AT) was obtained through BEI Resources, NIAID, NIH, and maintained in DMEM containing 10% FBS, 1% Pen/Strep, 1×NEAA, 1 g/mL puromycin (InVivogen, ant-pr-05).

The following SARS-CoV-2 strain/isolate was obtained through BEI Resources, NIAID, NIH: Washington strain 1 (WA1) (NR-52281). A recombinant virus expressing catalytic-inactive Nsp15 (Nsp15mut) was generated using an infection clone as described here (2). These viruses were propagated once with Vero-AT cells to obtain large viral stocks and were titrated with Vero-AT cells.

Assessment of Nsp15 activity inhibition with live SCoV-2

The evaluation of the inhibitory effect of Nsp15 inhibitors against live SARS-CoV-2 was conducted in a certified BSL-3 lab at Oklahoma State University. Caco2-AT cells ($3.0x10^5$ cells/well) were seeded in 12-well plates a day prior to infection. The work concentrations of the compounds were determined as follows based on a cell viability assay: P1A04, N1P21, and P1C04 at 0.5 mM; S7, S16, S17, and S24 at 0.1 mM; S9 and S21 at 0.2 mM; and S14 at 0.05 mM. Cells in the 12-well plates were infected with the indicated viral strains at a multiplicity of infection (MOI) of 0.1 in serum-free media for 1 hour. After incubation, the inoculum was removed, and 1 mL of diluted compound and 2 M p-glycoprotein inhibitor CP-100356 were added to each well. After 48 hours of incubation at 37°C, the cell culture supernatants were removed, and the cells were collected in Qiagen RLT lysis buffer (Qiagen, Hilden, Germany).

RNA extraction and Real-time PCR quantification

RNA was extracted from the Caco2-AT cells using RNeasy Mini kit (QIAGEN, 74106) following the manufacturer's protocol. 1 g of RNA was converted to cDNA by using RT2 HT First Strand Kit (QIAGEN, 330411) which contains a component to eliminate genomic DNA contamination. Quantitative PCR was performed with specific primers (Table S1) using PowerUp SYBR Green Master mix (Fisher, A25918) on QuanStudio 6 Pro (ThermoFisher, A43160). Cycle threshold values were normalized to 18S rRNA levels by using the 2^{-Ct} method. The forward and reverse primers for the human IFN- gene were CTTGGATTC-CTACAAAGAAGCAGC and TCCTCCTTCTGGAACTGCTGCA, respectively. The forward and reverse primers for the SARS-CoV-2 N gene were AAGCTGGACTTCCCTATG-GTG and CGATTGCAGCATTGTTAGCAGG, respectively.

Mass spectrometry

1D model

Mass spectrometry was performed at the Proteomics/ Mass Spectrometry Laboratory at the University of California, Berkeley. A nano LC column was packed in a 100-m inner diameter glass capillary with an integrated pulled emitter tip. The column consisted of 10 cm of Polaris c18 5-m packing material (Varian). The column was loaded and conditioned using a pressure bomb. The column was then coupled to an electrospray ionization source mounted on a Thermo-Fisher LTQ XL linear ion trap mass spectrometer. An Agilent 1200 HPLC equipped with a split line to deliver a flow rate of 1 µl/min was used for chromatography. Peptides were eluted with a 90-minute gradient from 100% buffer A (5% acetonitrile/0.02% heptafluorobutyric acid (HBFA)) to 60% buffer B (80% acetonitrile/0.02% HBFA). Collision-induced dissociation and electron transfer dissociation spectra were collected for each *m/z*. Protein identification and quantification and analysis were done with Integrated Proteomics Pipeline-IP2 (Bruker Scientific LLC, Billerica, MA, http://www.bruker.com)) using ProLuCID/Sequest[38, 39], DTASelect2[40, 41], and Census[42, 43].

Spectrum raw files were extracted into ms1 and ms2 files from raw files using RawExtract 1.9.9 (http://fields.scripps.edu/downloads.php) 10, and the tandem mass spectra were searched against Nsp15.

LC/MS-MS mapping of modified peptides

Trypsin/Lys-C digested peptides were analyzed by online capillary nanoLC-MS/MS using a 25 cm reversed-phase column fabricated in-house (75 µm inner diameter, packed with ReproSil-Gold C18-1.9 m resin (Dr. Maisch GmbH)) that was equipped with a laser-pulled nanoelectrospray emitter tip. Peptides were eluted at a flow rate of 300 nL/min using a linear gradient of 2–40% buffer B in 140 min (buffer A: 0.02% HFBA and 5% acetonitrile in water; buffer B: 0.02% HFBA and 80% acetonitrile in water) in a Thermo Fisher Easy-nLC1200 nanoLC system. Peptides were ionized using a FLEX ion source (Thermo Fisher) using electrospray ionization into a Fusion Lumos Tribrid Orbitrap Mass Spectrometer (Thermo Fisher Scientific). Data was acquired in orbi-trap mode. Instrument method parameters were as follows: MS1 resolution, 120,000 at 200 m/z; scan range, 3501600 m/z. The top 20 most abundant ions were subjected to collision-induced dissociation with a normalized collision energy of 35%, activation q 0.25, and precursor isolation width 2 m/z. Dynamic exclusion was enabled with a repeat count of 1, a repeat duration of 30 seconds, and an exclusion duration of 20 seconds. RAW files were analyzed using PEAKS (Bioinformatics Solution Inc.) with the following parameters: semi-specific cleavage specificity at the C-terminal site of R and K, allowing for 5 missed cleavages, precursor mass tolerance of 15 ppm, and fragment ion mass tolerance of 0.5 Daltons. Methionine oxidation was set as a variable modification and Cysteine carbamidomethylation was set as a fixed modification. Peptide hits were filtered using a 5% FDR. Proteins with at least 2 unique peptides were filtered with a 5% FDR. Label-free quantitation (LFQ) was performed using the PEAKS quantitation module and default parameters with the following exceptions: Top 2 peptides for each protein with a min of 10XE4 abundance was used and the TIC was used for all normalization including technical replicates.

Molecular modelling

The crystal structure of Nsp15 was obtained from the Protein Data Bank (PDB ID: 6WXC)[44]. The protein structure was prepared using the Maestro Schrödinger Protein Preparation Wizard. The co-crystallized ligand was removed, water molecules located more than 5 Å away from the protein residues were removed, missing side chains were added, and the pKa of the ionizable groups was set to 7.4 using PROPKA[45]. The protein then underwent restrained minimization and was placed inside an orthorhombic box. Water molecules (TIP3P) were added with a 10 Å buffer. The simulations were performed under the NPT ensemble to maintain a constant temperature and pressure, set at 300 K and 1.01325 bar, respectively, for 150 nanoseconds using the OPLS3 force field[46]. Separately, ligand molecules were prepared using the LigPrep module and then covalently bonded to cys293. The simulation outputs

were analyzed using the Schrödinger Maestro suite, with graphical representations created using ChimeraX[47, 48].

Drug-likeness evaluation

A list of SMILES of Nsp15 inhibitors that have IC_{50} less than 5 µM were submitted to a freely accessible web tool at SwissADME (http://www.swissadme.ch/http://www.swissadme.ch) and run.

4.5 Conclusions

Inhibition of Nsp15 has great potential for improving the treatment of SCoV-2. Nsp15 is a crucial endoribonuclease present in all coronaviruses that evades the immune response from the host during viral infection. Nsp15 suppresses the production of interferons by infected cells by cleaving the viral RNA. Down-regulating the production of interferons by SCoV-2 infected could have synergistic effects with inhibiting viral replication because it will prevent neighboring cells from being infected with viruses. Despite its potential, developing inhibitors against Nsp15 has been challenging due to large binding interface. HTS against SCoV-2 Nsp15 have yielded very few inhibitors, however, they are promiscuous hits. These hit compounds still require optimization to improve the inhibitory activity in virus-infected cells.

Cysteine reactive acrylamide compounds have shown great success as covalent inhibitors of proteins, especially making proteins undruggable to druggable. Here, we took this opportunity to screen never been never-explored acrylamide-based library against Nsp15. In this report, we screened a 2640 acrylamide-based electrophile library and identified ten cysteine reactive inhibitors against Nsp15 with IC_{50}s in the low micromolar range (less than 5 µM). These compounds have high reactivity towards free thiols to react with Nsp15 and are non-toxic in mammalian cells. Acrylamide-based inhibitors are specific to Nsp15 and could be utilized as initial hits for targeting other coronaviruses. The covalent linkage of compound 10 to Cys293 distorted the active, presence in the C-domain of Nsp15. Additionally, these compounds show drug-like properties including low molecular weight (180-300 g/mol), logP (less than 3), zero violations of Lipinski's rule, and no PAINS alert. Collectively, these results demonstrate that acrylamide fragments are a promising class of compounds for developing Nsp15 inhibitors and their optimal physiochemical and drug-likeness properties highlight its great potential for optimizing and developing into promising antiviral drug candidates. In conclusion, we present acrylamide-based covalent inhibitors against Nsp15 that could act as stepping stones for optimization to improve the inhibitory activity in virus-infected cells.

4.6 References

1. Y. Zhu, J. Li and Z. Pang, *Asian Journal of Pharmaceutical Sciences*, 2021, **16**, 4-23.

2. C. Pozzi, A. Vanet, V. Francesconi, L. Tagliazucchi, G. Tassone, A. Venturelli, F. Spyrakis, M. Mazzorana, M. P. Costi and M. Tonelli, *Journal of Medicinal Chemistry*, 2023, **66**, 3664-3702.

3. I. Pauly, A. Kumar Singh, A. Kumar, Y. Singh, S. Thareja, M. A. Kamal, A. Verma and P. Kumar, *Curr Pharm Des*, 2022, **28**, 3677-3705.

4. S. M. R. Hashemian, A. Sheida, M. Taghizadieh, M. Y. Memar, M. R. Hamblin, H. Bannazadeh Baghi, J. Sadri Nahand, Z. Asemi and H. Mirzaei, *Biomed Pharmacother*, 2023, **162**, 114367.

5. J. Liu, X. Pan, S. Zhang, M. Li, K. Ma, C. Fan, Y. Lv, X. Guan, Y. Yang and X. Ye, *The Lancet Regional Health–Western Pacific*, 2023, **33**.

6. Y. Duan, H. Zhou, X. Liu, S. Iketani, M. Lin, X. Zhang, Q. Bian, H. Wang, H. Sun, S. J. Hong, B. Culbertson, H. Mohri, M. I. Luck, Y. Zhu, X. Liu, Y. Lu, X. Yang, K. Yang, Y. Sabo, A. Chavez, S. P. Goff, Z. Rao, D. D. Ho and H. Yang, *Nature*, 2023, **622**, 376-382.

7. S. A. Moghadasi, E. Heilmann, A. M. Khalil, C. Nnabuife, F. L. Kearns, C. Ye, S. N. Moraes, F. Costacurta, M. A. Esler, H. Aihara, D. von Laer, L. Martinez-Sobrido, T. Palzkill, R. E. Amaro and R. S. Harris, *Sci Adv*, 2023, **9**, eade8778.

8. X. Deng, M. Hackbart, R. C. Mettelman, A. O'Brien, A. M. Mielech, G. Yi, C. C. Kao and S. C. Baker, *Proc Natl Acad Sci U S A*, 2017, **114**, E4251-E4260.

9. E. Kindler, C. Gil-Cruz, J. Spanier, Y. Li, J. Wilhelm, H. H. Rabouw, R. Zust, M. Hwang, P. V'Kovski, H. Stalder, S. Marti, M. Habjan, L. Cervantes-Barragan, R. Elliot, N. Karl, C. Gaughan, F. J. van Kuppeveld, R. H. Silverman, M. Keller, B. Ludewig, C. C. Bergmann, J. Ziebuhr, S. R. Weiss, U. Kalinke and V. Thiel, *PLoS Pathog*, 2017, **13**, e1006195.

10. D. Zhang, L. Ji, X. Chen, Y. He, Y. Sun, L. Ji, T. Zhang, Q. Shen, X. Wang, Y. Wang, S. Yang, W. Zhang and C. Zhou, *iScience*, 2023, **26**, 107705.

11. C. K. Yuen, J. Y. Lam, W. M. Wong, L. F. Mak, X. Wang, H. Chu, J. P. Cai, D. Y. Jin, K. K. To, J. F. Chan, K. Y. Yuen and K. H. Kok, *Emerg Microbes Infect*, 2020, **9**, 1418-1428.

12. C. J. Otter, N. Bracci, N. A. Parenti, C. Ye, L. H. Tan, A. Asthana, J. J. Pfannenstiel, N. Jackson, A. R. Fehr, R. H. Silverman, N. A. Cohen, L. Martinez-Sobrido and S. R. Weiss, *bioRxiv*, 2023, DOI: 10.1101/2023.11.15.566945.

13. M. C. Pillon, M. N. Frazier, L. B. Dillard, J. G. Williams, S. Kocaman, J. M. Krahn, L. Perera, C. K. Hayne, J. Gordon, Z. D. Stewart, M. Sobhany, L. J. Deterding, A. L. Hsu, V. P. Dandey, M. J. Borgnia and R. E. Stanley, *Nat Commun*, 2021, **12**, 636.

14. M. N. Frazier, I. M. Wilson, J. M. Krahn, K. J. Butay, L. B. Dillard, M. J. Borgnia and R. E. Stanley, *Nucleic Acids Res*, 2022, **50**, 8290-8301.

15. J. Chen, R. Abou Farraj, D. Limonta, S. A. T. Dakhili, E. M. Kerek, A. Bhattacharya, F. M. Reformat, O. M. Mabrouk, B. Brigant and T. A. Pfeifer, *Journal of Biological Chemistry*, 2023, **299**.

16. F. Sutanto, M. Konstantinidou and A. Dömling, *RSC Med Chem*, 2020, **11**, 876-884.

17. P. Ábrányi-Balogh, L. Petri, T. Imre, P. Szijj, A. Scarpino, M. Hrast, A. Mitrović, U. P. Fonovič, K. Németh, H. Barreteau, D. I. Roper, K. Horváti, G. G. Ferenczy, J. Kos, J. Ilaš, S. Gobec and G. M. Keserű, *Eur J Med Chem*, 2018, **160**, 94-107.

18. A. O. Walter, R. T. T. Sjin, H. J. Haringsma, K. Ohashi, J. Sun, K. Lee, A. Dubrovskiy, M. Labenski, Z. Zhu and Z. Wang, *Cancer discovery*, 2013, **3**, 1404-1415.

19. M. S. Davids and J. R. Brown, *Future Oncol*, 2014, **10**, 957-967.

20. B. A. Lanman, J. R. Allen, J. G. Allen, A. K. Amegadzie, K. S. Ashton, S. K. Booker, J. J. Chen, N. Chen, M. J. Frohn and G. Goodman, *Journal*, 2019.

21. L. Boike, N. J. Henning and D. K. Nomura, *Nature Reviews Drug Discovery*, 2022, **21**, 881-898.

22. S. Wang, Y. Tian, M. Wang, M. Wang, G. B. Sun and X. B. Sun, *Front Pharmacol*, 2018, **9**, 353.

23. R. Choi, M. Zhou, R. Shek, J. W. Wilson, L. Tillery, J. K. Craig, I. A. Salukhe, S. E. Hickson, N. Kumar, R. M. James, G. W. Buchko, R. Wu, S. Huff, T. T. Nguyen, B. L. Hurst, S. Cherry, L. K. Barrett, J. L. Hyde and W. C. Van Voorhis, *PLoS One*, 2021, **16**, e0250019.

24. E. Resnick, A. Bradley, J. Gan, A. Douangamath, T. Krojer, R. Sethi, P. P. Geurink, A. Aimon, G. Amitai, D. Bellini, J. Bennett, M. Fairhead, O. Fedorov, R. Gabizon, J. Gan, J. Guo, A. Plotnikov, N. Reznik, G. F. Ruda, L. Díaz-Sáez, V. M. Straub, T. Szommer, S. Velupillai, D. Zaidman, Y. Zhang, A. R. Coker, C. G. Dowson, H. M. Barr, C. Wang, K. V. M. Huber, P. E. Brennan, H. Ovaa, F. von Delft and N. London, *J Am Chem Soc*, 2019, **141**, 8951-8968.

25. S. Parasuraman, *J Pharmacol Pharmacother*, 2011, **2**, 74-79.

26. R. C. Borra, M. A. Lotufo, S. M. Gagioti, M. Barros Fde and P. M. Andrade, *Braz Oral Res*, 2009, **23**, 255-262.

27. A. Reichel and P. Lienau, *Handb Exp Pharmacol*, 2016, **232**, 235-260.

28. A. Daina, O. Michielin and V. Zoete, *Scientific Reports*, 2017, **7**, 42717.

29. B. Bakchi, A. D. Krishna, E. Sreecharan, V. B. J. Ganesh, M. Niharika, S. Maharshi, S. B. Puttagunta, D. K. Sigalapalli, R. R. Bhandare and A. B. Shaik, *Journal of Molecular Structure*, 2022, **1259**, 132712.

30. S. B. Bunally, C. N. Luscombe and R. J. Young, *SLAS Discovery*, 2019, **24**, 791-801.

31. A. T. Garcia-Sosa, U. Maran and C. Hetenyi, *Curr Med Chem*, 2012, **19**, 1646-1662.

32. D. F. Veber, S. R. Johnson, H.-Y. Cheng, B. R. Smith, K. W. Ward and K. D. Kopple, *Journal of Medicinal Chemistry*, 2002, **45**, 2615-2623.

33. A. Daina and V. Zoete, *ChemMedChem*, 2016, **11**, 1117-1121.

34. F. Protti Í, D. R. Rodrigues, S. K. Fonseca, R. J. Alves, R. B. de Oliveira and V. G. Maltarollo, *ChemMedChem*, 2021, **16**, 1446-1456.

35. C. A. Lipinski, F. Lombardo, B. W. Dominy and P. J. Feeney, *Adv Drug Deliv Rev*, 2001, **46**, 3-26.

36. Y. C. Martin, *J Med Chem*, 2005, **48**, 3164-3170.

37. E. Şahin, A. Karanfil, M. Çol Ayvaz and E. Şahin, *Journal of Molecular Structure*, 2021, **1248**, 131357.

38. T. Xu, J. D. Venable, S. K. Park, D. Cociorva, B. Lu, L. Liao, J. Wohlschlegel, J. Hewel and J. Yates, *Mol. Cell. Proteomics*, 2006, **5**, S174.

39. T. Xu, S. K. Park, J. D. Venable, J. A. Wohlschlegel, J. K. Diedrich, D. Cociorva, B. Lu, L. Liao, J. Hewel, X. Han, C. C. L. Wong, B. Fonslow, C. Delahunty, Y. Gao, H. Shah and J. R. Yates, 3rd, *J Proteomics*, 2015, **129**, 16-24.

40. D. Cociorva, D. Tabb and J. Yates, *Current protocols in bioinformatics / editoral board, Andreas D. Baxevanis ... [et al.]*, 2007, **Chapter 13**, Unit 13.14.

41. D. L. Tabb, W. H. McDonald and J. R. Yates, 3rd, *J Proteome Res*, 2002, **1**, 21-26.

42. S. K. Park, J. D. Venable, T. Xu and J. R. Yates, *Nature Methods*, 2008, **5**, 319-322.

43. S. K. R. Park, A. Aslanian, D. B. McClatchy, X. Han, H. Shah, M. Singh, N. Rauniyar, J. J. Moresco, A. F. M. Pinto, J. K. Diedrich, C. Delahunty and J. R. Yates, III, *Bioinformatics*, 2014, **30**, 2208-2209.

44. Y. Kim, J. Wower, N. Maltseva, C. Chang, R. Jedrzejczak, M. Wilamowski, S. Kang, V. Nicolaescu, G. Randall, K. Michalska and A. Joachimiak, *Commun Biol*, 2021, **4**, 193.

45. C. R. Søndergaard, M. H. Olsson, M. Rostkowski and J. H. Jensen, *J Chem Theory Comput*, 2011, **7**, 2284-2295.

46. K. Roos, C. Wu, W. Damm, M. Reboul, J. M. Stevenson, C. Lu, M. K. Dahlgren, S. Mondal, W. Chen, L. Wang, R. Abel, R. A. Friesner and E. D. Harder, *J Chem Theory Comput*, 2019, **15**, 1863-1874.

47. E. C. Meng, T. D. Goddard, E. F. Pettersen, G. S. Couch, Z. J. Pearson, J. H. Morris and T. E. Ferrin, *Protein Sci*, 2023, **32**, e4792.

48. E. F. Pettersen, T. D. Goddard, C. C. Huang, E. C. Meng, G. S. Couch, T. I. Croll, J. H. Morris and T. E. Ferrin, *Protein Sci*, 2021, **30**, 70-82.

4.7 Acknowledgments

I acknowledge all advisors and researchers, Niren Murthy, Daniel K. Nomura, Lydia H. Zhang and Lauren M. Orr, Robin Stanley and Huanchen Wang, Basil P. Hubbard and Evan M. Kerek, Xufang Deng and Xueying Liang, Seyed Amir Tabatabael Dakhili, Julia Schaletzky and Eddie Wehri, Silin Guo, Rushil N. Desai, for supporting this project in numerous ways including, conceiving this project, screening of chemical libraries, validating the hits, specificity assays, cellular assays, computational efforts, high throughput screening, performing assays, respectively.

This chapter is being used for preparing a manuscript, entitled Identification of Acrylamide-based covalent inhibitors of SARS-CoV-2 (SCoV-2) Nsp15 using high-throughput screening.

Chapter 5

Conclusions and Future Directions

The emergence of SCoV-2 has necessitated a rapid and effective response in drug discovery, focusing on targeting viral proteins essential for the viral replication and survival. Among these, PLpro (papain-like protease)[1] and Nsp15 (non-structural protein 15)[2] have garnered significant attention due to their crucial roles in viral RNA processing and immune evasion, respectively. PLpro is attractive target due to its dual function in processing the viral polyprotein and modulating the immune response from host. Small molecule inhibitors of PLpro have shown promise in preclinical studies, effectively blocking the protease activity and restoring the host immune response.[3] Nsp15, an endoribonuclease, is vital for the virus to evade the host immune response by degrading viral RNA intermediates that would otherwise trigger antiviral defenses. Inhibition of Nsp15 has shown the potential to reduce the viral infection. Small molecules that could disrupt the endonuclease activity of Nsp15, could act as its inhibitor, thereby enhancing the immune response against the virus. [4]

In conclusion, small molecule inhibitors targeting Nsp15 and PLpro represent a promising avenue in the fight against COVID-19. The successful development of these inhibitors could provide effective therapeutic options to reduce viral load and improve patient outcomes. Ongoing research and optimization efforts are essential to overcome the existing challenges and ensure the rapid translation of these inhibitors from the laboratory to clinical use. The lessons learned from this drug discovery process will also be invaluable in preparing for future pandemics, highlighting the importance of a robust and agile approach to antiviral drug development.

Small molecule inhibitors targeting these proteins represent promising therapeutic strategies to mitigate the impact of COVID-19. However, PLpro and Nsp15 are not easy to drug target[5, 6]. In the case of PLpro, the structural studies have provided insights into the binding mechanisms of these inhibitors, guiding the design of more potent and specific compounds. Most of the covalent inhibitors are based on the GRL0617 (non-covalent inhibitor as a parent compound), could lead to drug resistance[6]. To meet the unmet need of discovering new parent compound, we found a reversible covalent inhibitor (based on mercaptopyrimidine ring) against PLpro that inhibited SCoV-2 replication.[7] Whereas, in the case of Nsp15, it is a very challenging to drug due to its complex structure and size[5]. Research has identified several

potential Nsp15 inhibitors through virtual screening, biochemical assays, and structural biology techniques. These inhibitors have demonstrated efficacy in inhibiting Nsp15 activity, leading to reduced viral replication *in vitro*. However, these compounds are hydrophobic, aromatic in nature that could bind to non-specific proteins as well. These promiscuous compounds require the continued optimization of these molecules, focusing on improving their potency, selectivity, and pharmacokinetic properties, is critical for developing a viable therapeutic option. In our study, we screened an acrylamide-based electrophile library to discover covalent inhibitors against Nsp15.

The drug discovery process for Nsp15 and PLpro inhibitors has been accelerated by advances in computational modeling, high-throughput screening, and structure-based drug design. Virtual screening of large compound libraries, followed by biochemical validation, has led to the identification of several lead compounds. Crystallographic studies have further elucidated the interaction between these inhibitors and their target proteins, enabling rational modifications to enhance efficacy. These efforts highlight the importance of an integrated approach combining computational, biochemical, and structural biology techniques in the discovery and optimization of antiviral drugs.

Despite the progress, several challenges remain in the development of Nsp15 and PLpro inhibitors. Ensuring the specificity of these inhibitors to avoid off-target effects and minimizing potential toxicity are critical hurdles.[8] Additionally, the emergence of viral mutations may affect the binding efficacy of these inhibitors, necessitating continuous monitoring and adaptation of the drug candidates. Addressing these challenges requires a concerted effort from the scientific community, leveraging collaborative research and sharing of data to expedite the drug development process.

The future of drug discovery, particularly focusing on small molecule inhibitors targeting Nsp15 and PLpro in SCoV-2[9, 10], represents a promising and dynamic field within the broader context of COVID-19 therapeutics. The lessons learned from the pandemic have accelerated scientific innovation and collaboration, laying a robust foundation for more efficient and effective drug development processes. This essay explores the advancements and future directions in drug discovery for Nsp15 and PLpro inhibitors, as well as the overall landscape of COVID-19 drug discovery.

In conclusion, the future of drug discovery for small molecule inhibitors targeting Nsp15 and PLpro, as well as broader COVID-19 therapeutics, is bright. Driven by technological advancements, a deeper understanding of viral biology, and enhanced global collaboration, these efforts will lead to more effective and efficient therapeutic solutions. The integration of AI, high-throughput screening, structural biology, and collaborative research will be key to overcoming current challenges and realizing the full potential of these therapeutic strategies[11]. These advancements will not only provide effective treatments for COVID-19 but also contribute to a broader framework for antiviral drug development, ultimately enhancing global health security and preparedness for future pandemics.

5.1 References

1. Y. M. Báez-Santos, S. E. St John and A. D. Mesecar, *Antiviral Res*, 2015, **115**, 21-38.

2. M. C. Pillon, M. N. Frazier, L. B. Dillard, J. G. Williams, S. Kocaman, J. M. Krahn, L. Perera, C. K. Hayne, J. Gordon, Z. D. Stewart, M. Sobhany, L. J. Deterding, A. L. Hsu, V. P. Dandey, M. J. Borgnia and R. E. Stanley, *Nat Commun*, 2021, **12**, 636.

3. D. J. Calleja, G. Lessene and D. Komander, *Front Chem*, 2022, **10**, 876212.

4. M. Saramago, V. G. Costa, C. S. Souza, C. Bárria, S. Domingues, S. C. Viegas, D. Lousa, C. M. Soares, C. M. Arraiano and R. G. Matos, *Microorganisms*, 2022, **10**.

5. J. Chen, R. A. Farraj, D. Limonta, S. A. Tabatabaei Dakhili, E. M. Kerek, A. Bhattacharya, F. M. Reformat, O. M. Mabrouk, B. Brigant, T. A. Pfeifer, M. T. McDermott, J. R. Ussher, T. C. Hobman, J. N. M. Glover and B. P. Hubbard, *J Biol Chem*, 2023, **299**, 105341.

6. B. C. Sanders, S. Pokhrel, A. D. Labbe, I. I. Mathews, C. J. Cooper, R. B. Davidson, G. Phillips, K. L. Weiss, Q. Zhang, H. O'Neill, M. Kaur, J. G. Schmidt, W. Reichard, S. Surendranathan, J. Parvathareddy, L. Phillips, C. Rainville, D. E. Sterner, D. Kumaran, B. Andi, G. Babnigg, N. W. Moriarty, P. D. Adams, A. Joachimiak, B. L. Hurst, S. Kumar, T. R. Butt, C. B. Jonsson, L. Ferrins, S. Wakatsuki, S. Galanie, M. S. Head and J. M. Parks, *Nature Communications*, 2023, **14**, 1733.

7. T. Bajaj, E. Wehri, R. K. Suryawanshi, E. King, K. S. Pardeshi, K. Behrouzi, Z. Khodabakhshi, U. Schulze-Gahmen, G. R. Kumar, M. R. K. Mofrad, D. K. Nomura, M. Ott, J. Schaletzky and N. Murthy, *RSC Advances*, 2023, **13**, 17667-17677.

8. B. Van Loy, A. Stevaert and L. Naesens, *Antiviral Res*, 2024, **228**, 105921.

9. S. Lei, X. Chen, J. Wu, X. Duan and K. Men, *Signal Transduction and Targeted Therapy*, 2022, **7**, 387.

10. B. Canal, R. Fujisawa, A. W. McClure, T. D. Deegan, M. Wu, R. Ulferts, F. Weissmann, L. S. Drury, A. P. Bertolin, J. Zeng, R. Beale, M. Howell, K. Labib and J. F. X. Diffley, *Biochem J*, 2021, **478**, 2465-2479.

11. A. I. Visan and I. Negut, *Life (Basel)*, 2024, **14**.